Departamento de Engenharia Eletrotécnica e de Computadores

VALIDAÇÃO EXPERIMENTAL DE TÉCNICAS DE COMPENSAÇÃO DE EFEITOS NÃO LINEARES EM SISTEMAS RÁDIO OFDM SOBRE FIBRA

Gonçalo Rafael de Mesquita Argel

VOLUME 1

Dissertação no âmbito do Mestrado Integrado em Engenharia Eletrotécnica e de Computadores do ramo de Telecomunicações orientada pela Professora Doutora Maria do Carmo Raposo Medeiros e apresentada ao Departamento de Engenharia Eletrotécnica e de Computadores.

Setembro de 2018

UNIVERSIDADE D
COIMBRA

Department of Electrical and Computer Engineering

EXPERIMENTAL VALIDATION OF NONLINEAR EFFECTS COMPENSATION TECHNIQUES IN OFDM RADIO OVER FIBER SYSTEMS

Gonçalo Rafael de Mesquita Argel

VOLUME 1

Dissertation in the scope of the Integrated Master in Electrical and Computer Engineering of the Telecommunications branch guided by Ph.D. Professor Maria do Carmo Raposo Medeiros and presented to the Department of Electrical and Computer Engineering.

September of 2018

UNIVERSIDADE D
COIMBRA

The work developed in this dissertation was carried out within the framework of the projects Project UID/EEA/50008, sub-project PhoTech-5G/60GH, RETIOT, SAICT-45-2015-03 Project nº 16432, and supported by the IT infrastructure facilities namely the ORCIP Centro-01-0145-FEDER-002141.

AGRADECIMENTOS

À minha orientadora, Professora Doutora Maria do Carmo Raposo Medeiros, por me acolher neste projeto e pelo apoio e disponibilidade demonstrados.

À minha colega Beatriz Oliveira, por toda a dedicação e por estar sempre disposta a ajudar.

À minha família por estar sempre presente, incentivando-me a continuar a trabalhar e a percorrer este percurso tão gratificante. Uma referência especial ao meu pai, o meu pilar, e à minha irmã gémea, a minha outra metade.

Aos meus amigos, correndo o risco de me tornar redundante, pois são a família que escolhi. Por todas as vivências partilhadas, pelo companheirismo constante e inúmeros sorrisos que me proporcionam.

RESUMO

Atualmente, a utilização de serviços de comunicação é indispensável, exigindo um aumento na taxa de transmissão e da qualidade do serviço (QoS). Devido ao crescimento exponencial dos produtos e do número de utilizadores, é expectável que no futuro a comunicação *wireless* terá que lidar com o congestionamento nas baixas frequências. Por esta razão, estão a ser realizados estudos nas ondas milimétricas com especial ênfase na banda não licenciada 60GHz, particularmente destinada a aplicações redes locais (WLAN), tendo em vista a próxima geração de comunicação *wireless* - 5G. A arquitetura C-RAN (*Centralized Radio Acces Network*) é uma estratégia promissora para ultrapassar o problema do congestionamento da banda e da taxa de transmissão. Nesta abordagem, todas as funcionalidades de processamento são transferidas das estações base (*base stations* [BSs]) para a designada unidade central [*central unit* (CU)], e as estações base são substituídas por antenas remotas [*remote radio heads* (RRHs)], reduzindo o custo da rede. A ligação entre as CU e as RRHs é feita através de ligações de fibra ótica (*radio over fiber* [RoF]). Apesar dos sistemas de comunicação por fibra ótica permitirem uma maior largura de banda e poucas perdas em relação aos cabos coaxiais, eles introduzem distorção nos sinais de rádio frequência.

Para atenuar a distorção causada pela ligação RoF que interliga as CU e as RHHS, foram propostas técnicas de pré-distorção baseadas em algoritmos de polinómios de memória. O seu desempenho foi analisado num ambiente de simulação.

Esta dissertação valida experimentalmente a melhoria de desempenho alcançada quando a pré-distorção é aplicada num sistema RoF que utiliza modulação OFDM (*Orthogonal Frequency-Division Multiplexing*). O trabalho está dividido em duas partes. A primeira consiste na análise de um sistema de transmissão OFDM, sendo identificadas e discutidas as suas limitações em termos de ordem de constelação. Na segunda parte, a ligação eletro-ótica é adicionada ao sistema e a função de pré-distorção é implementada e as melhorias no seu desempenho são analisadas e discutidas.

Palavras-Chave: Rádio sobre Fibra (RoF), Orthogonal Frequency-Division Multiplexing (OFDM), Rádio, Compensação de distorção, Polinómios de Memória.

ABSTRACT

Nowadays the use of communication services is indispensable, requiring the increase of data rate and quality of service (QoS). Due to the exponential growth of products and number of users, is expected that in the future wireless communication will have to deal with a congestion in low frequencies. For this reason, studies are being carried out for the next generation of wireless communication, 5G, at millimeter-waves with special focus in the unlicensed 60 GHz band, particularly aimed for indoor applications. Centralized radio access network (C-RAN) architecture is a promising strategy to overcome the congestion and data rate problem. In this approach, the baseband processing and radio functionalities are moved from the base stations (BSs) to a called central unit (CU) and the base stations are replaced by remote antennas (remote radio heads [RRHs]), which reduce the cost of the network. The connection between the CU and the RRHs is made through radio over fiber (RoF) optical fiber links. Despite the fact that optical fiber links have higher bandwidth and few losses when compared with coaxial cables, they introduce distortion in the radio signals.

To mitigate the distortion introduced by the RoF link that connects the CU and the RHHs, pre-distortion techniques based on memory polynomial algorithms have been proposed and their performance analyzed in a simulation environment.

This dissertation validates experimentally, the performance improvement achieved when pre-distortion is employed in a RoF system that employs orthogonal frequency-division modulation (OFDM). The work is divided into two parts. The first consists in the analysis of an OFDM transmission system, being identified and discussed its limitations in terms of constellation order. In the second one, the electro-optical link is added to the system and the predistortion function is implemented in the system and the improvement in its performance is analyzed and discussed.

Keywords: Radio over Fiber (RoF), Orthogonal Frequency-Division Multiplexing (OFDM), Distortion compensation, Memory polynomials.

CONTENTS

LIST OF FIGURES

LIST OF TABLES

LIST OF ACRONYMS

1G	1st Generation
2G	2nd Generation
3G	3rd Generation
5G	5th Generation
A-RoF	Analog Radio over Fiber
ADC	Analog to Digital Converter
BBU	Base Band Unit
BER	Bit Error Rate
BS	Base Station
C-RAN	Centralized Radio Access Network
CFO	Carrier Frequency
CP	Cyclic Prefix
CU	Central Unit
D-RoF	Digital Radio over Fiber
DAC	Digital to Analog Converter
DFT	Discrete Fourier Transform
DML	Directly Modulated Laser
E/O	Electrical to Optical Converter
EOPM	Electro-Optic Phase Modulator
EVM	Error Vector Magnitude
FDM	Frequency Division Multiplexing
FDMA	Frequency Division Multiple Access
FFT	Fast Fourier Transform
FMT	Filtered Multi-Tone Transmission
Fs	Sample Frequency
GSM	Global System for Mobile Communications
ICI	Inter -Carrier Frequency

IDFT	Inverse Discrete Fourier Transform
IF	Intermediate Frequency
IFFT	Inverse Fast Fourier Transform
IMD	Intermodulation Distortions
IMPs	Intermodulation Products
IQ	Quadrate
ISI	Inter-Symbol Interference
LPF	Low-Pass Filter
MBH	Mobile Backhaul
MFH	Mobile Fronthaul
mm-Wave	Millimeter Wave
MNOs	Mobile Network Operators
MSC	Mobile Switch Center
MZIM	Mach-Zehnder Intensity Modulator
MZM	Mach-Zehnder Modulator
O/E	Optical to Electrical Converter
OA	Optical Amplifier
OFDM	Orthogonal Frequency Division Multiplexing
OH	Hydroxyl groups
P/S	Parallel to Serial Converter
PA	Power Amplifier
PAM	Pulse Amplitude Modulation
PAPR	Peak-to-Average Power Ratio
PD	Photodetector
PSK	Phase Shift Keying
QAM	Quadrature Amplitude Modulation
QoS	Quality of Service
RAN	Radio Access Network
RC	Raise Cosine
RF	Radio Frequency
RHH	Remote Radio Head
RI	Refractive Index
RoF	Radio over Fiber

RU	Radio Unit
S/P	Serial to Parallel Converter
SRRC	Square Root Raise Cosine
STO	Symbol Time Offset
TDMA	Time Division Multiple Access
WLAN	Wireless Local Network
ZP	Zero Padding

CHAPTER 1 – INTRODUCTION

1.1 CONTEXT AND MOTIVATION

A few years ago, scientific community predicted that by now the wireless traffic volume would be huge when compared to the existing one, and the data rate would be 10 to 100 times superior with low latency requirements [1]. This trend does not seem to slow down, considering that the pace of technological development has grown exponentially year by year. It is estimated that in a near future the spectrum up to 10GHz will be congested. A solution to avoid spectrum congestion has been the topic of study of several researchers. One approach that is considered reliable is the shift to the millimeter wave spectrum, more precisely, for indoor application, to the 60 GHz unlicensed band that provides a multi-giga communication services. There are already some standards for wireless local networks (WLAN) developed for this millimeter-wave (mm-wave) band such as IEEE 802.15.3c and IEE.802.11ad [2]. For these reasons it is expected that 60 GHz band will have an important role for the 5th generation (5G) mobile networks. However, mm-waves have significant propagation issues, including atmospheric and rain absorption, low diffraction, which leads to blockage sensitivity. Moreover, mm-waves are extremely directional, and need to employ beamforming techniques. These drawbacks impose a limitation on wireless propagation distance, which implies an increase in the number of remote radio heads (RRHs). Studies are being carried out for the past years in order to improve the radio over fiber (RoF) link in the distribution of these RRHs systems [3].

The exponential growth of the wireless traffic volume also brings another bottleneck to the existing network architecture, since the increase of the number of users represent a need to deploy more BSs. Consequently, the energy consumption and the infrastructure costs would increase. Therefore, a new strategy for 5G architecture emerged: Centralized radio access network (C-RAN). The concept of this configuration is to create a centralization of the signal processing. In other words, the central unit (CU) includes the digital

to analog converter (DAC), the analog to digital converter (ADC) and all processing functionalities, whereas the RRHs only contain the optical to electrical (O/E) and electrical to optical (E/O) converters, amplifiers and antennas. The connection between the CU and the RRHs is made by a RoF link. Despite of the advantages that RoF technology brings, its optoelectronic devices introduce nonlinear distortions, to which RF signals, such as orthogonal frequency division multiplexing (OFDM) signal, are very sensitive. A strategy to compensate the non-linearity effects involves the implementation of a predistortion algorithm [4].

1.2 OBJECTIVES

The main goal of this dissertation is the experimental validation of the compensation of the RoF system nonlinearities by means of predistortion implemented in [3]. The experimental validation methodology will be divided in two parts. In first place, a study of the limitations of the OFDM system transmission in terms of constellation order will be carried out, according with the variation of certain parameters such as number of carriers, number of OFDM symbols and samples per symbol of the filter, which directly affect the bit rate. It will also be chosen an intermediate frequency (IF) to carry the OFDM signal. This study is helpful to select reliable parameters for the second part. Here, the OFDM signal modulates a continuous wave (CW) by means of a Single-Driver Mach-Zehnder Intensity Modulator. The distortions introduced by the RoF link are identified and characterized, and the improvement of system performance with predistortion algorithm developed in [3] is analyzed.

1.3 STRUCTURE

After the contextualization of this dissertation, chapter 2 will present the evolution of the mobile network architecture in direction of C-RAN and the RoF technologies used to transmit wireless signals. Following this, chapter 3 gives an overview of the OFDM radio signal. It is also made a description of the transmission scheme and its components, an identification of OFDM drawbacks and a brief note of the system assessment metrics.

In order to introduce the RoF experimental scheme, chapter 4 brings out the RoF system model, introducing the RoF link and the up-conversion system. It is also identified the nonlinear distortions imposed by each optical component, the figures of merit used to characterize these distortions and how they can be compensated.

Chapter 5 takes care of the experimental validation, which is the focus of this dissertation. The experimental setups and procedures are presented, as well as the characteristics of the components used. The characterization of the nonlinear distortions is also presented for different levels of signal amplitude. To end the chapter, the implementation of predistortion is accomplished by means of the predistortion coefficients optimization and its application to the OFDM signal. The results are presented and discussed.

Lastly, in chapter 6, present conclusions and future work suggestions.

1.4 MAIN CONTRIBUTIONS

The main contribution of this dissertation is the experimental validation of the pre-distortion method developed in [3] for certain OFDM parameters. In this dissertation it was developed all the software necessary to support the experimental set-up. The software models developed and implemented were:

- Matlab function to generate and save in ".txt" OFDM signal
- Matlab function to transpose a generated data to the 25 GHz
- Matlab function to receive the OFDM signal from the scope and calculate the predistortion coefficients based on memory polynomials
- Matlab function to generate OFDM signal and apply the predistortion coefficients
- Matlab function to receive the predistorted signal from the scope and characterize the improvement accomplished with predistortion

It was also prepared a user manual, that includes all the necessary steps to upload the signal to the signal generator used (AT-AWG-GS 2500).

CHAPTER 2 – MOBILE FRONTHAUL OVERVIEW

The objective of this chapter is to provide an overview of the cellular base station architecture towards a C-RAN. The different segments of the architecture are identified, namely the mobile backhaul (MB), the mobile fronthaul (MF) and the access network. RoF technology is identified as an innovative technology to support the MF [5].

2.1 CELLULAR BASE STATION ARCHITECTURAL EVOLUTION

2.1.1 TRADITIONAL RADIO ACCESS NETWORK (RAN)

A traditional radio access network (RAN) called Macro Base Station (MBS), as shown in Fig. 1, was used in 1G and 2G mobile networks and comprises stand-alone BSs two electronic subsystems: a radio unit (RU) and a radio equipment controller (REC), also known as base band unit (BBU). The RU is responsible for the transmission and processing of the RF signal, whereas the BBU process baseband, i.e., it's in charge of the communication through the physical interface. These were usually located in a dedicated room at the base of the tower or in a building. The connection between the RU and the antennas was made by heavy and large diameters coaxial cables. BS covers a cell, and is responsible for processing, transmitting and receiving signals to and from all mobile terminals in the BS coverage range. The cell sites are connected with the wireless core network mobile switching center (MSC) through packet switched backhaul networks. This

architecture has high deployment costs, large equipment footprint and high power consumption.

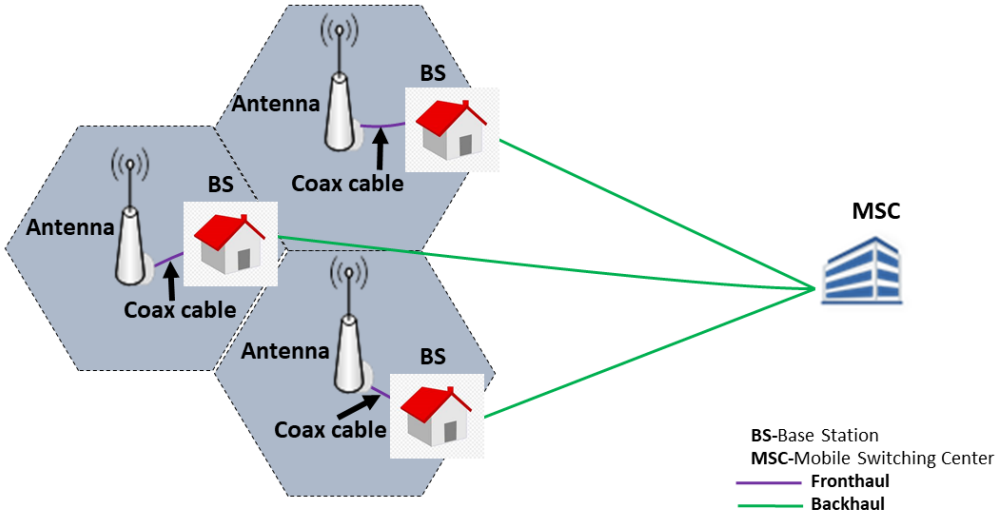

FIGURE 1 - TRADITIONAL RADIO ACCESS NETWORK (RAN). SOURCE: [13]

2.1.2 DISTRIBUTED BS ARCHITECTURE

For 3G, a new version of traditional MBS (Fig. 2) was introduced by a leading telecom equipment vendors group. In this architecture the BBU and RU or RRH are separated using a fiber connection instead of copper cabling; although, microwaves connection can also be applied. This replacement leads to considerable improvements such as wider network coverage, low power requirements, higher bandwidth, reduction of noise and also allows that BBU and RRHs can be placed a hundred meters or kilometers away [5]. This improved version of conventional MBS also installed the RRH near the antennas, which helps to reduce the power consumption and losses in the RF signal.

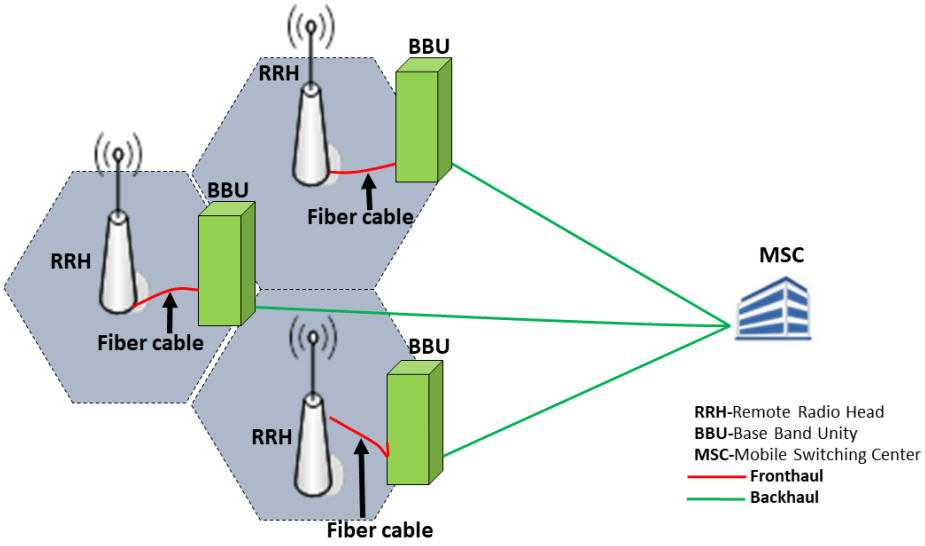

FIGURE 2 - DISTRIBUTED BS ARCHITECTURE. SOURCE: [13]

2.1.3 CENTRALIZED RAN (C-RAN)

Mobile Network Operators (MNOs) felt the need to improve the existent architecture due to the increase of communications users and applications, because this growth implies also a rise on the number of BS and, consequently, more energy consumption. The principle of the upgrade version of this configuration, C-RAN, is to move the BBUs from the BSs to the MSC, creating the so-called BBU centralization. Therefore, the BS turns into a simple RRH, which can be set on lampposts or rooftops, resulting in an efficient cooling system and reduction in energy expenditure. The connection between the BBU and the core network is identified as Mobile Backhaul (MBH), whereas the BBU-RRH link is called Mobile Fronthaul (MFH). Due to the centralization processing, other advantages emerge, such as the mitigation of inter-cell interference. A schematic figure of this architecture is shown in Fig. 3.

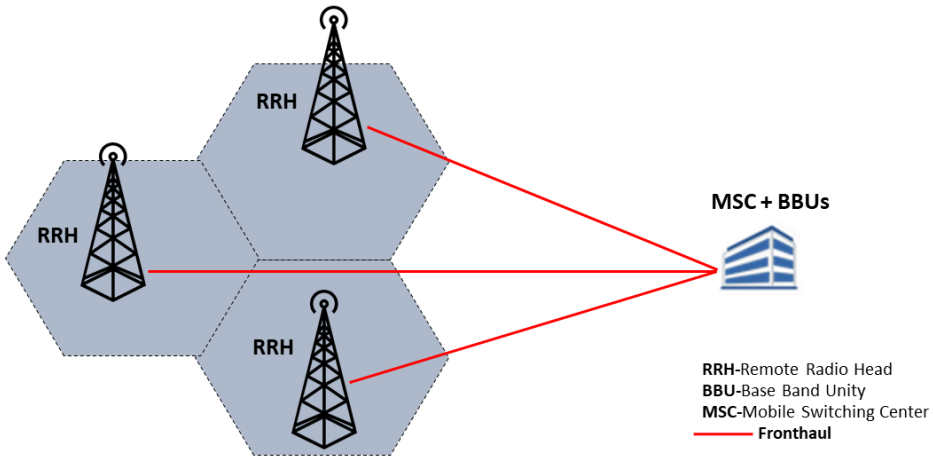

FIGURE 3 - CENTRALIZED RAN (C-RAN). SOURCE: [13]

2.3 RoF TECHNOLOGIES

2.3.1 ANALOG RoF

The analog RoF (A-RoF) modulate directly the optical carrier with microwave signal. This modulation can be implemented with modulated lasers (DMLs) for low frequencies, whereas, for higher frequencies, external modulators are required, such as MZM. In an A-RoF transmission, because there is no up/down RF conversion, the system only needs the optical modulator at the transmitter and a PD at the receiver. However, with multi-carrier RF systems, such as OFDM system, the RoF link suffers from inter-modulation distortions (IMD) introduced by nonlinearity of both RF and optical components. Moreover, optical fiber chromatic dispersion and attenuation, that increases with the fiber length, also contribute to the degradation of the link and limitation of the dynamic range [5].

2.3.2 DIGITIZED ROF

Contrary to A-RoF, the Digitized RoF (D-RoF) move the Analog to Digital Converter (ADC) and Digital to Analog Converter (DAC) functions to the RRH. With this approach, the laser is directly modulated by the digital signal, which mitigates the non-linear effects presented in A-RoF transmission. Therefore, the dynamic range of the system is independent of the fiber length. Furthermore, this configuration turns the CU simpler and enable a higher perfomance at RRHs. However, it brings other issues such as aliasing, quantization and an increase in the number of circuit elements.

2.4 ANALOG VERSUS DIGITIZED ROF

Since the general consensus is that from 4G to 5G the network capacity will increase by roughly 1000× [6] . This makes 5G backhaul a key technical challenge. Therefore, in the fronthaul section of the network, digitalization of the wireless signal is not a good option, since heavy signal processing would be necessary at the RRHs, which would increase complexity, power consumption and add extra network latency the RRH. Therefore, the strategy that will be studied in this dissertation, for the fronthaul, is the transmission of the RF signals, more specifically OFDM signals, in their native format, by external modulation of an optical carrier through a single-drive Mach-Zehnder intensity modulator (MZIM).

CHAPTER 3 – OFDM OVERVIEW

In this chapter, only the electrical part of the RoF system is considered, i.e., the OFDM transmission system. Initially, OFDM is introduced. In section 3.2 an OFDM system scheme and its components are presented. Then, section 3.3 gives a general idea of the OFDM drawbacks. Another major issue – intermodulation distortions (IMD) – is introduced in section 3.4. The chapter ends with an identification of the performance assessment metrics used.

3.1 INTRODUCTION TO OFDM

3.1.1 SINGLE-CARRIER VS MULTI-CARRIER TRANSMISSION

High data rate transmission over mobile or wireless channels is required by many applications. In order to support the symbol rate (R_s), the minimum required bandwidth is the Nyquist bandwidth, which is given by $R_s/2$. Therefore, a broader bandwidth is required to support a higher data rate, in a single-carrier transmission system (Fig. 4), such as Time-Division Multiple Access (TDMA) or Global System for Mobile Communications (GSM). Furthermore, when the signal bandwidth becomes larger than the coherence bandwidth in the wireless channel, the link suffers from multi-path fading, incurring the inter-symbol interference (ISI). In general, adaptive equalizers are employed to deal with ISI. However, the complexity of an equalizer increases with the data rate so as the ISI. The growth of the complexity is due to the fact that the inverse function becomes sharper as the frequency-selectivity of the channel increases [7].

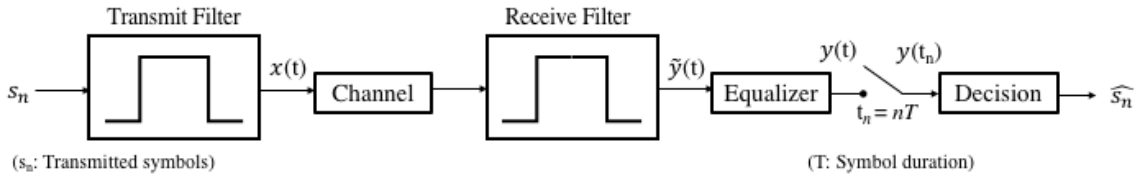

FIGURE 4 - SINGLE-CARRIER TRANSMISSION SYSTEM. SOURCE: [7]

To overcome the frequency selectivity problem in single-carrier transmission, multiple carriers can be used. In a multi-carrier transmission system (Fig. 5), a wideband signal is analyzed into several narrowband signals at the transmitter and synthesized at the receiver so that the frequency-selective wideband channel can be approximated by multiple frequency-flat narrowband channels. This method is denominated as frequency non-selectivity and reduces the complexity of the equalizer for each subchannel.

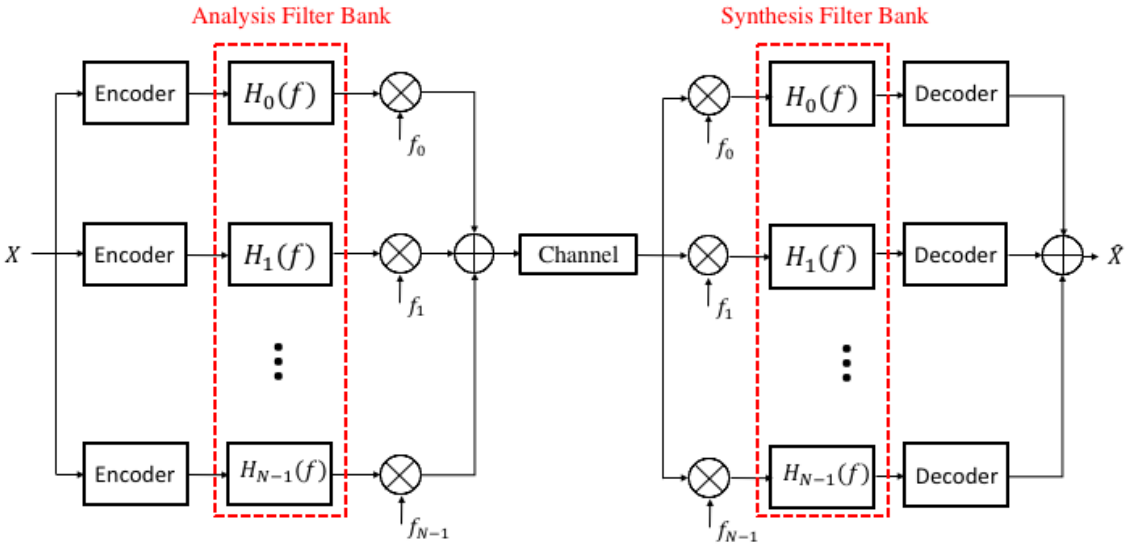

FIGURE 5 - MULTI-CARRIER TRANSMISSION SYSTEM. SOURCE: [7]

In a classical parallel data system, such as Filtered Multi-Tone Transmission (FMT), the bandwidth is divided into nonoverlapping frequency subchannels, each having a subcarrier frequency, whereupon the signal is centered (Fig. 6). This means that multi-carrier transmission can be seen as a Frequency Division Multiple Access (FDMA).

For better understanding of the differences between single and multi-carrier transmissions in a few words, a single fade or interference may cause the entire link to fail in a single-carrier system, whereas, in a multi-carrier system only a few subchannels will be affected, which can be corrected with error correction coding.

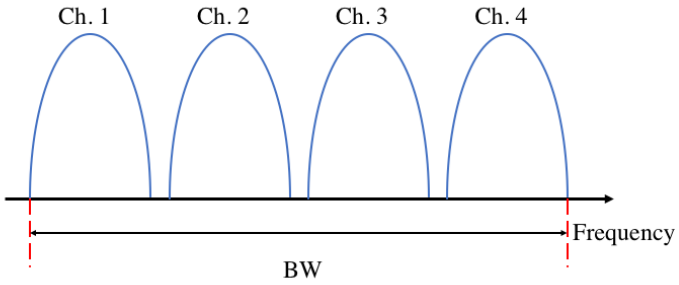

FIGURA 6 – TRADITIONAL MULTICARRIER SYSTEM. SOURCE: [8]

3.1.2 OFDM (DEFINITION)

Another type of multi-carrier transmission system is the Orthogonal Frequency Division Multiplexing (OFDM). Unlike an FDM system, OFDM subcarriers are overlapped. As the Fig. 7 indicates, using this technique it is possible to reduce the bandwidth usage nearly 50%. However, with the overlapping of the subcarrier Inter-Carrier Interference (ICI) increases. Therefore, as the name indicates, they need to be mutually orthogonal. This orthogonality is accomplished in practice using Discrete Fourier Transform (DFT) and Inverse Discrete Fourier Transform (IDFT), which, in turn, are implemented by Fast Fourier Transform (FFT) and Inverse Fast Fourier Transform (IFFT). To deal with the ISI effect over the multipath channel, in the OFDM system is implemented a

guard interval. Under certain conditions, that will be presented in the next section of this chapter, the ISI and/or ICI can be reduced almost entirely.

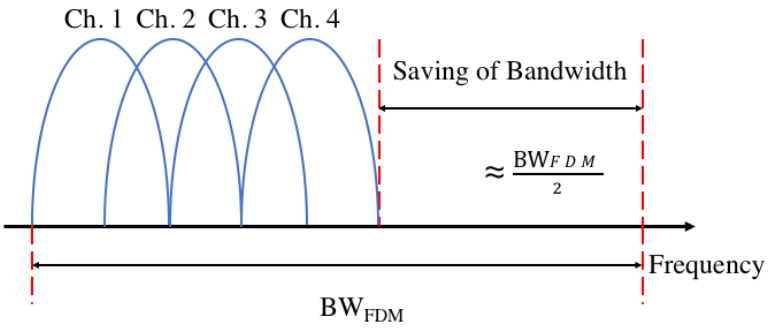

FIGURE 7 - ORTHOGONAL FREQUENCY DIVISION MULTIPLEXING (OFDM). SOURCE: [8]

Despite of the OFDM system be advantageous in many ways, it has also drawbacks. Due to the overlapping of the subcarrier, OFDM is more sensitive to frequency offset and phase noise and has a considerable peak-to-average power ratio, which reduce the power efficiency of the RF amplifier.

3.1.2.1 GUARD INTERVAL

The OFDM guard interval can be added in two different ways: Cyclic Prefix (CP) or Zero Padding (ZP). CP is the cyclic extension of the OFDM symbol copying the last samples of the symbol to its front (Fig. 8). The duration of the OFDM symbol is now $T_{sym} = T_s + T_{CP}$, where T_s is the symbol duration with guard interval and T_{CP} is the duration of the cyclic prefix. To mitigate the ISI and ICI effects and maintain the orthogonality the length of the CP must be longer than the maximum delay of the multipath channel.

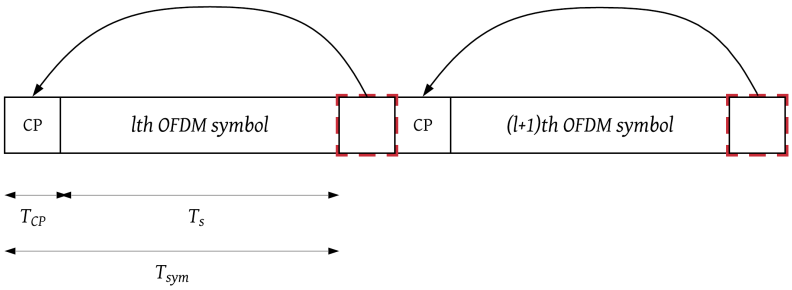

FIGURE 8 – CYCLIC PREFIX METHOD. SOURCE: [7]

The other way of a use a guard interval is to insert zeros in the same condition as the one mention before (ZP). However, even under this condition a small symbol time offset may occur. Thus, the guard interval of the next OFDM symbol is copied and added into the head part of the current symbol to avoid the ICI, as shown in Fig. 9.

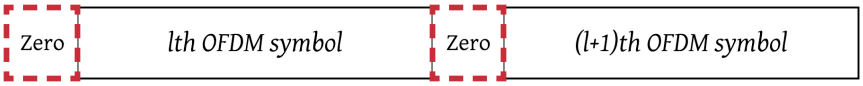

FIGURE 9 – ZERO PADDING METHOD. SOURCE: [7]

3.2 OFDM TRANSMISSION SYSTEM

The structure of the transmitter and receiver of an OFDM system are represented in Fig. 10. The binary data is first mapped into a sequence of M-Quadrature Amplitude Modulation (M-QAM) or M-Phase Shift Keying (M-PSK) (will not be used in the system implemented) symbols, which will be converted from serial to N parallel blocks. Each one of them is carried out by a different subcarrier.

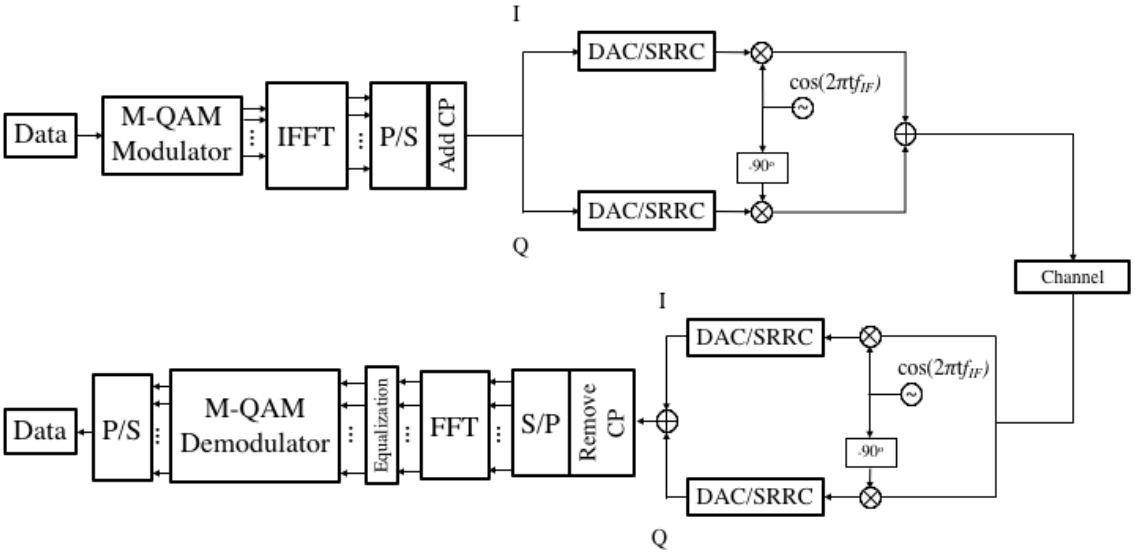

FIGURE 10 - OFDM TRANSMISSION SCHEME. SOURCE: [7]

Due to the serial to parallel (S/P) conversion, the duration of transmission time (T_s) is extended according with the number of symbols N, creating a single OFDM symbol with a length of $T_{sym} = \mathrm{N}T_s$ [7]. Consider $X_l[k]$ the l^{th} transmit symbol at k^{th} subcarrier, with $l = 0,1,2,\dots,\infty$ and $k = 0,1,2,\dots,N-1$, and $\Psi_{l,k}(t)$ the l^{th} OFDM signal at the k^{th} sub-carrier, which is given as

$$\Psi_{l,k}(t) = \begin{cases} e^{j2\pi f_k(t-lT_{sym})}, & 0 < t \leq T_{sym} \\ 0, & otherwise \end{cases} \quad (1)$$

Thus, the passband OFDM signal, in the continuous-time domain can be defined as

$$x_l(t) = Re\left\{\frac{1}{T_{sym}}\sum_{l=0}^{\infty}\sum_{k=0}^{N-1} X_l[k].\Psi_{l,k}(t)\right\} \tag{2}$$

and the baseband OFDM signal as

$$x_l(t) = \frac{1}{T_{sym}}\sum_{l=0}^{\infty}\sum_{k=0}^{N-1} X_l[k]e^{j2\pi f_k(t-lT_{sym})} \tag{3}$$

The baseband OFDM signal being sampled at $t = lT_{sym} + nT_s$, with $T_s = T_{sym}/N$ and $f_k = k/T_{sym}$, becomes the N-point IDFT of PSK or QAM data symbols and can be computed efficiently by using the IFFT. The discrete-time OFDM signal can be expressed as

$$x_l[n] = \sum_{k=0}^{N-1} X_l[k]e^{j2\pi kn/N} \tag{4}$$

After the IFFT process, the signal is converted to serial and the CP is added. After that, the data is converted to the analog domain by using a DAC. A Square Root Raised Cosine (SRRC) is used as Low-Pass Filter (LPF) to mitigate the aliasing components inserted by the DAC. The final process of the OFDM transmitter is up-convert the OFDM signal to a carrier frequency f_{IF}, using a quadrature (IQ) modulator. In a similar way, the received discrete-time OFDM symbol is denoted as $y_l[n]$, then the received OFDM signal is given as

$$Y_l[k] = \sum_{n=0}^{N-1} y_l[n]e^{-j2\pi kn/N} \tag{5}$$

At the receiver, are applied the reverse operations, yet an equalizer is implemented after the FFT block in order to compensate the error in amplitude and phase.

3.2.1 **M**-ARY **Q**UADRATURE **A**MPLITUDE **M**ODULATION

OFDM transmitter, as is depicted in Fig. 10, convert the bits into a sequence of M-ary PSK or QAM symbols before the OFDM modulation. In this dissertation only the M-QAM Modulator and Demodulator (at the receiver) were used. M-ary QAM systems are a two-dimensional generalization of M-ary PAM (Pulse Amplitude Modulation), i.e., two orthogonal PAM signals are transmitted on the same channel by quadrature-carrier multiplexing, without require more bandwidth. One of the signals represents the in-phase component and the other the quadrature component:

$$\psi_1(t) = \sqrt{\frac{2}{T}}\cos(2\pi f_c t)\ , \quad 0 \le t \le T \tag{6}$$

$$\psi_2(t) = \sqrt{\frac{2}{T}}\operatorname{sen}(2\pi f_c t)\ , \quad 0 \le t \le T. \tag{7}$$

Considering the constellation point ($\psi_1\,\psi_2$ plane) denoted as ($a_i d_{min}/2$, $b_i d_{min}/2$), where d_{min} represents the minimum distance between two constellations points. In its turn, $d_{min}/2 = \sqrt{E_0}$, which is the square root of half the energy of the point closest to the origin of the axes. The QAM signal can be express in terms of $\psi_1(t)$ and $\psi_2(t)$ as

$$s_i = a_i\sqrt{E_0}\,\psi_1(t) + b_i\sqrt{E_0}\,\psi_2(t)\,, \tag{8}$$
$$i = -L+1, \ldots, -1, 0, 1, L-1, \text{ with } L = \sqrt{M}.$$

Fig. 11 shows the rectangular constellations of 4-QAM (or Quadrature Phase Shift Keying-QPSK), 16-QAM, 64-QAM and 256-QAM. Note that they are not normalized.

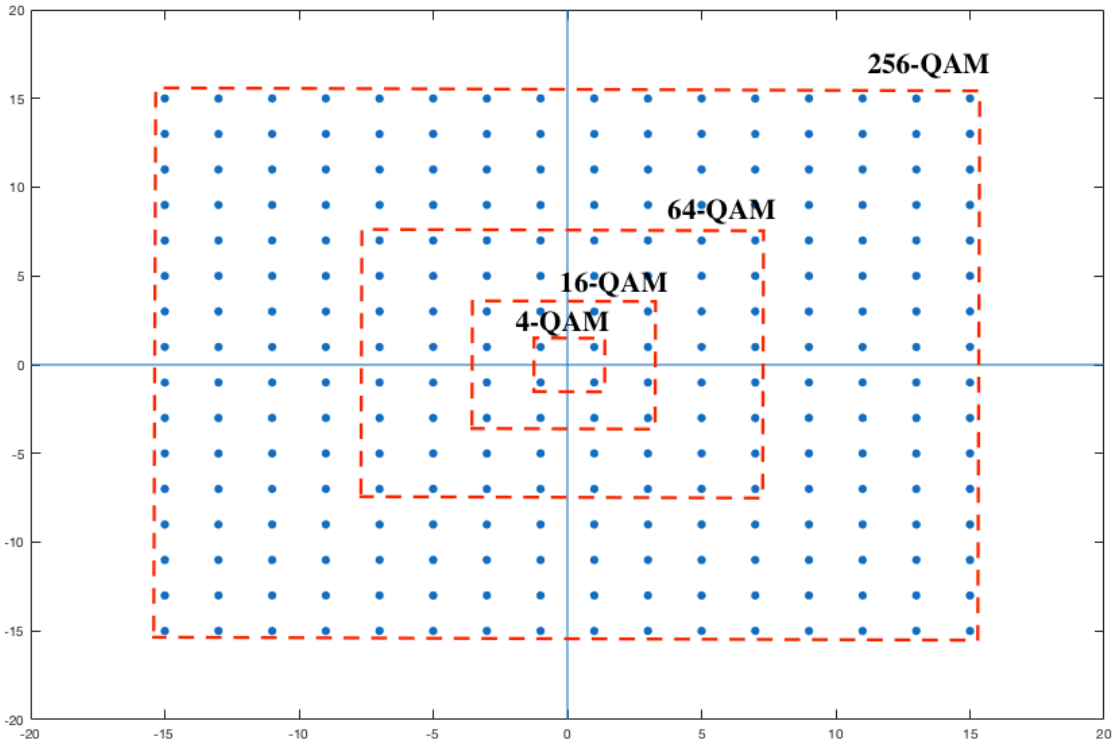

FIGURE 11 – QAM CONSTELLATIONS DIAGRAM

An illustrative example of QAM modulator and demodulator scheme is presented on the figures below, respectively:

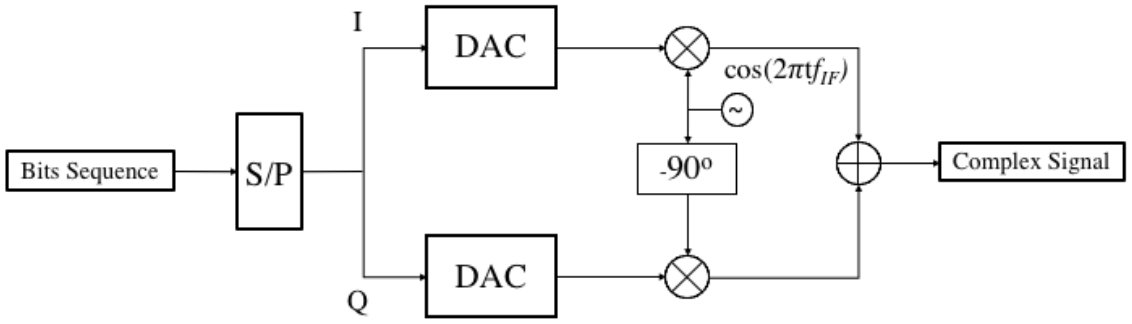

FIGURE 12 - QAM MODULATOR

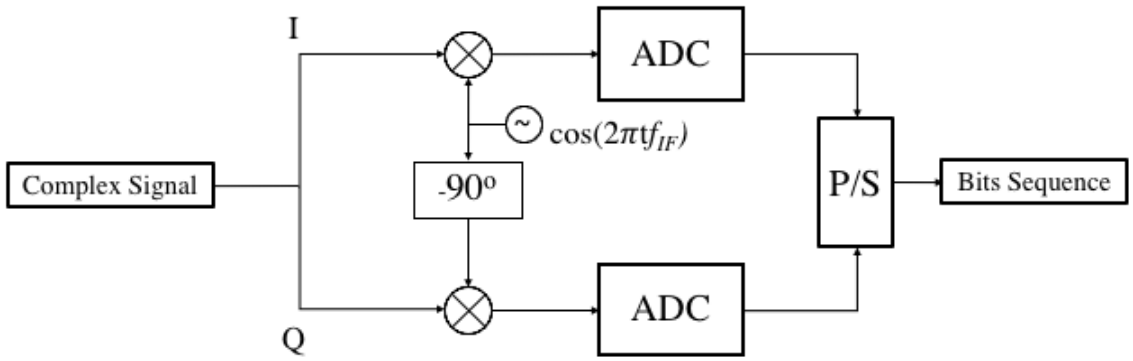

FIGURE 13 - QAM DEMODULATOR

3.2.2 RAISED COSINE FILTER

As shown in the transmission system scheme, both the transmitter and the receiver have a SRRC in order to the overall filtering be a raised cosine (RC) response, which can be expressed as

$$H(f) = \begin{cases} 1, & |f| \leq \frac{1-\beta}{2T} \\ \frac{1}{2}\left[1 + \cos\left(\frac{\pi T}{\beta}\left[|f| - \frac{1-\beta}{2T}\right]\right)\right], & \frac{1-\beta}{2T} < |f| \leq \frac{1+\beta}{2T} \\ 0, & otherwise \end{cases} \quad (9)$$

and its bandwidth as

$$BW = \frac{\beta + 1}{T} \ (Hz) \tag{10}$$

where T is the symbol duration, f the frequency vector and β the roll-off factor ($0 \leq \beta \leq 1$). As the equations shows, the roll-off factor shapes the filter and its bandwidth, so that the filter goes from rectangular ($\beta = 0$) to cosine ($\beta = 1$) and the bandwidth increases with β. This type of filtering is applied because its spectrum is a *sync* function with zero-crossing in multiples of T, mitigating the ISI effect.

3.2.3 EQUALIZER

As mention before, the Equalizer implemented in the receiver is used to compensate the distortion introduced by the channel in the frequency domain. This improvement is accomplished using training symbols, which are chosen in the beginning of the transmission. The first step of the equalization method is to calculate the transfer function by subcarrier. Each one is defined as

$$TF_{sys,k} = \frac{1}{N_t} \sum_{n=1}^{N_t} \frac{Y_{k,n}}{X_{k,n}} \tag{11}$$

After all transfer functions are calculated, each of their inverse is respectively applied to the received signal, concluding the equalization process.

3.3 DRAWBACKS

3.3.1 PEAK-TO-AVERAGE POWER RATIO (PAPR)

It is known that even linear amplifiers inflict nonlinear distortions due to their saturation characteristics. Since OFDM subcarriers are overlapped, in the time domain they are added causing high amplitude peaks. This amplitude peaks lead the system to operate under nonlinear conditions. Therefore, OFDM systems have a considerable Peak-to-Average Power Ratio (PAPR) problem. Denoting the transmitted signal as *s(t)*, PAPR is define as the ration between the maximum power and the average power of the pass-band signal:

$$PAPR = \frac{max\{|s(t)|^2\}}{E\{|s(t)|^2\}} \tag{12}$$

A meticulous study about this problem and its possible solutions has been made in [7].

3.3.2 PHASE NOISE AND FREQUENCY OFFSET

In the OFDM receiver there are two principal distortions related with the carrier frequency: phase noise and frequency offset. For the demodulation process, the receiver needs to know the exact number of samples of the transmitted signal, i.e., in order to the FFT function can be applied, the synchronization must be done in the starting point of each OFDM symbol; otherwise, the OFDM signal suffers a symbol time offset (STO). A STO in the time domain incurs in a phase offset in the frequency domain. Phase noise mainly affects the OFDM system in two different ways. The first is that insert a random phase variation, which is common to all carrier frequencies; yet, if the OFDM symbol rate is much bigger than the oscillator linewidth. This effect can be minimized through

tracking techniques or differential detection. The second and more notorious is that the subcarriers are no longer space by $1/T$ in the frequency domain, such that ICI occurs [8]. Carrier frequency offset (CFO) is caused by Doppler effect[1], beside the ineluctable physical differences of the oscillators. Doppler frequency shift f_d is given as

$$f_d = \frac{v\, f_c}{c} \tag{13}$$

where v is the velocity of the receiver, f_c is the carrier frequency in the transmitter and c is the speed of light [7]. If a frequency offset occurs, the number of cycles in the FFT window is no longer an integer, which leads to appearance of ICI after the FFT. The ICI effect is more glaring for subcarriers in the middle of the OFDM spectrum than for the subcarriers at the bandwidth brinks [8].

3.4 INTERMODULATION DISTORTION

Another big drawback of OFDM systems is the sensitivity to nonlinear distortion in the RF transmissions, mainly caused by the power amplifiers (PA). In practice, the nonlinear properties of the PA introduce intermodulation products (IMPs), which increase the distortion in OFDM signal band and causes interference to neighbor channels. IMPs also appears in the harmonic frequencies of the signal; however, those are easily removed by filters since they are outside of the transmission band. To demonstrate the effect of intermodulation distortion, let denote a signal with two carriers as $s(t)$, which is defined as

$$s(t) = \cos(2\pi f_1 t) + \cos(2\pi f_2 t) \tag{14}$$

and the transfer function of the non-linear system as

[1] An explanation of the Doppler effect is made in [14]

$$h(x) = a_1 s(t) + a_2 s^2(t) + a_3 s^3(t) \quad (15)$$

Expanding and collecting terms, the output will be

$$y(t) = a_2 \quad \textbf{DC terms} \quad (16)$$

$$+\left[a_1 + \frac{3}{2}a_3 + \frac{9}{4}a_3\right] \times [\cos(2\pi f_1 t) + \cos(2\pi f_2 t)] \textbf{Fundamental terms}$$

$$+\frac{1}{2}a_2[\cos(2\pi(2f_1)t) + \cos(2\pi(2f_2)t)] \quad \textbf{2nd harmonic terms}$$

$$+ a_2[\cos(2\pi(f_1 + f_2)t) + \cos(2\pi(f_1 + f_2)t)] \quad \textbf{2nd order products}$$

$$+\frac{1}{4}a_3[\cos(2\pi(3f_1)t) + \cos(2\pi(3f_2)t)] \quad \textbf{3rd harmonic terms}$$

$$+\frac{3}{4}a_3[\cos(2\pi(2f_1 + f_2)t) + \cos(2\pi(2f_2 + f_1)t)] \textbf{3rd order products}$$
$$+\frac{3}{4}a_3[\cos(2\pi(2f_1 - f_2)t) + \cos(2\pi(2f_2 - f_1)t)]$$

It can be seen that emerge new components in the transmitted signal. The fundamental terms are now affected by coefficients a_1 and a_3. Considering that f_1 and f_2 (as they should in a communication system), the 3rd order products at frequencies $(2f_1 - f_2)$ and $(2f_2 - f_1)$ lie inside of the transmission band, which will cause several interferences at the receiver. The other generated signal components will be filtered or out of band [9]. Below are illustrated the IMPs (Fig. 14).

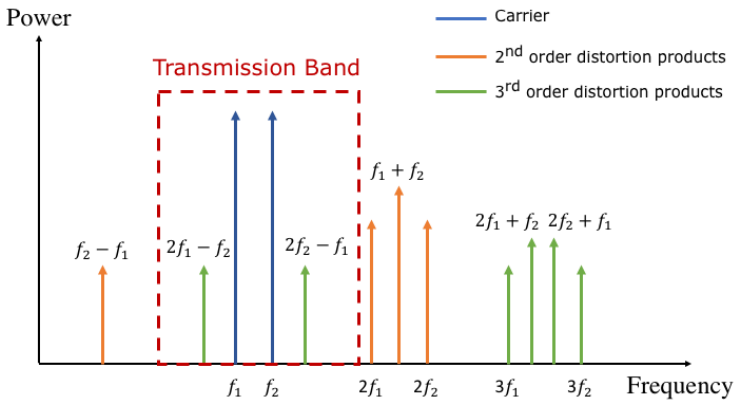

FIGURE 14 – ILUSTRATION OF INTERMODULATION DISTORTIONS

3.5 PERFORMANCE ASSESSMENT METRICS

3.5.1 ERROR VECTOR MAGNITUDE

Error Vector Magnitude (EVM) is a measurement to assess the system performance in communication applications. It is a difference vector between the received signal and the ideal symbol, i.e., the symbol that would be received if there were no interference in the transmission channel. The EVM is typically expressed as a percent of the average power per symbol of the constellation:

$$\mathrm{EVM}_{rms}(\%) = \left[\frac{\frac{1}{N}\sum_{k=1}^{N} |Y_k - X_k|^2}{\frac{1}{N}\sum_{k=1}^{N} |X_k|^2} \right]^{\frac{1}{2}} \times 100 \qquad (17)$$

where $X_k = X_{I,k} + iX_{Q,k}$ is the ideal point of the constellation and $Y_k = Y_{I,k} + iY_{Q,k}$ is the received symbol.

3.5.2 BIT ERROR RATE

Bit Error Rate (BER) is a performance metric used in communication systems that depict the probability of error according to the number of incorrect bits. Considering that a M-ary modulation is used, the probability of error, P_b, can be express as [15]

$$P_b \approx \frac{2\left(1-\frac{1}{L}\right)}{\log_2 L} Q\left[\sqrt{\left(\frac{3\log_2 L}{L^2-1}\right)\frac{2E_b}{N_0}}\right] \tag{18}$$

where L is the number of levels in each dimension of M-ary modulation system, E_b is the energy per bit, $\frac{N_0}{2}$ is the noise power spectral density and Q is the Gaussian co-error function and is given as

$$Q(x) = \int_x^{\infty} \frac{1}{\sqrt{2\pi}} e^{\frac{-y^2}{2}} dy \tag{19}$$

Though, in order to set a relationship with the EVM, BER can be define as follows

$$P_b \approx \frac{2\left(1-\frac{1}{L}\right)}{\log_2 L} Q\left[\sqrt{\left(\frac{3\log_2 L}{L^2-1}\right)\frac{2}{EVM_{RMS}^2 \log_2 M}}\right] \tag{20}$$

where L and Q represents the same as above and M is the number of M-ary symbols transmitted.

CHAPTER 4 – ROF SYSTEM MODEL

This chapter starts with a brief contextualization of the RoF link, including optical up-conversion. The nonlinear distortions imposed by the optical components are identified. It is also presented a characterization of these distortions and the compensation method.

4.1 ROF LINK

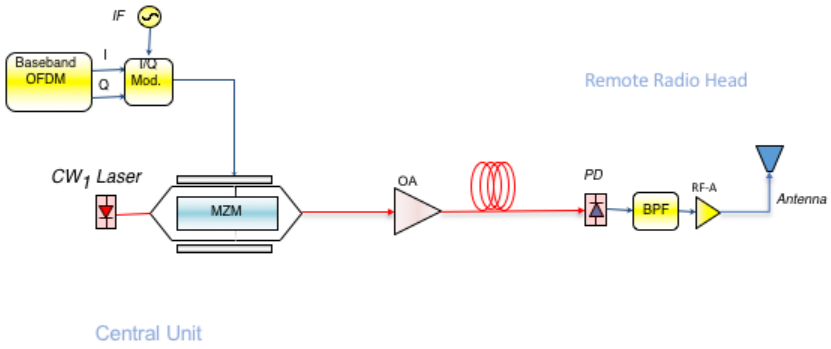

FIGURE 15 – SCHEMATIC ILLUSTRATION OF ROF LINK. SOURCE: [4]

A macro view of the system schematic is illustrated in Figure 15. A continuous wave (CW) laser is modulated by an OFDM signal located at the intermediate frequency, *IF*, by means of a Match Zehnder modulator (MZM). The OFDM signal is transmitted in the optical domain from the CU to the RRH. At the RRH, the optical signal is photo-detected and bandpass filtered to avoid unwanted components; the filtered signal is amplified by a RF power amplifier and irradiated by the transmitting antenna.

We can identify several limitations on this architecture:

a) Need for high frequency RF oscillators and mixers.
b) It is difficult to generate RF frequencies higher than 10 GHz. The conventional RF techniques used to generate mm-wave carriers rely on several stages of RF frequency multiplication or mixing which add excessive phase noise to the RF carrier.
c) Need for high bandwidth MZM. MZM with bandwidths higher than 10 GHz are very expensive.
d) The optical components and optical fiber introduce nonlinear distortion.

The a), b) and c) limitations can be overcome by using optical up-conversion strategies [11]. However, nonlinear distortions introduced by the optical link remains in the system. In order to demonstrate these distortions, a spectrum of experimental tests was collected and is shown in Fig. 16.

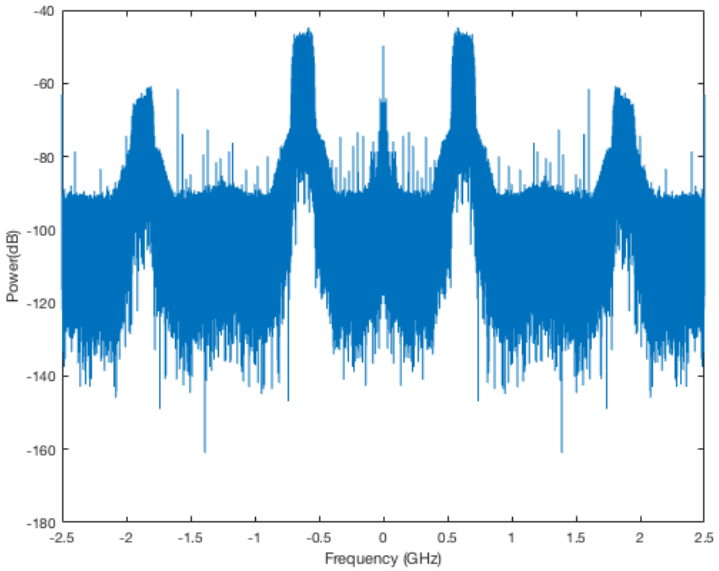

FIGURE 16: SPECTRUM COLLECTED DURING THE EXPERIMENTAL TESTS THAT ILUSTRATES IMDS

4.2 RoF LINK EMPLOYING OPTICAL UP-CONVERSION

A simple up-conversion strategies mixes, upon photodetection, a modulated optical carrier (the one at the output of MZM) and unmodulated optical carrier, generating the RF signal. The optical field of each carrier is, respectively, $E_1(t) = \sqrt{2P_1}e^{j(2\pi v_1 t+\theta_1(t))}$ and $E_2(t) = \sqrt{2P_2}e^{j(2\pi v_2 t+\theta_2(t))}$, where P_1 and P_2 are the respective optical powers, v_1 and v_2 the optical frequencies, $\theta_1(t)$ and $\theta_2(t)$ the instantaneous phases [3]. The generated photocurrent $I_{PD}(t)$ is given by,

$$I_{PD}(t) = \mathcal{R}|E_2(t) + E_1(t)|^2\, e^{j(2\pi(v_2-v_1)t+\theta_2(t)-\theta_1(t))} + \text{other terms} \qquad (21)$$

where $\mathcal{R}$ is the responsivity.

The mixing process leads to the generation of new components at the sum and difference of the two input frequencies, whereby the difference in frequency is set to be at the required RF carrier frequency, as shown in Fig. 17. However, this process is affected by the phase noise of the optical carriers and therefore only correlated optical sources upon photodetection produce spectrally pure RF carriers.

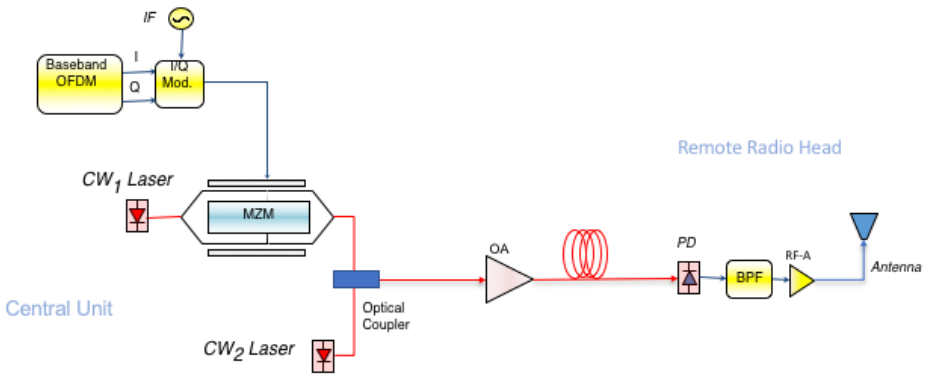

FIGURE 17 – ROF LINK EMPLOYING OPTICAL UP-CONVERSION. SOURCE: [4]

It is important to note, that optical up-conversion does not increase the nonlinear distortion of the system. Since the focus of this dissertation is the compensation of the nonlinear distortion, optical up-conversion will not be considered.

4.3 Nonlinear Distortion introduced by the RoF link

4.3.1 Single Drive Mach-Zehnder Intensity Modulator

As mention before, the electro-optic conversion can be accomplished by means of a Mach-Zehnder intensity modulator, shown in Fig. 18. The field of the optical waveguide at the input is equally split. Each arm of the MZIM is an electro-optic phase modulator (EOPM), used, as the name suggests, to modulate the phase of the optical carrier by means of a driving voltage, V_d. When this voltage is applied to the electrode of each arm separately, the refractive index (RI) of the waveguide changes and, consequently, the phase of the optical field as well. For other words, the phase of the optical field can be controlled by the driving voltage. The optical fields from the arms are summed up at the output [12].

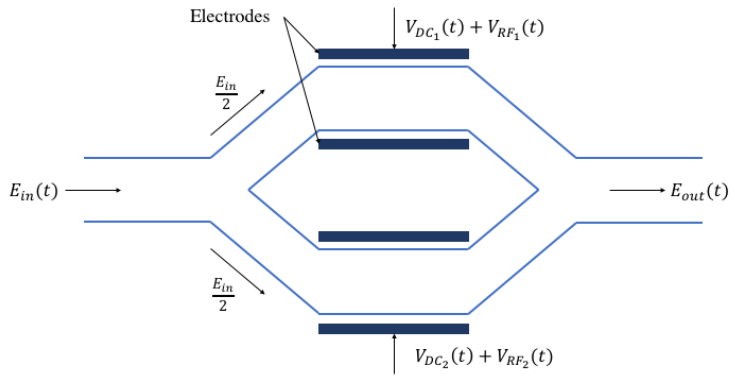

FIGURE 18 - MACH-ZEHNDER INTENSITY MODULATOR

The driving voltage is given as

$$V_{d_i} = V_{Dc_i} + V_{RF_i} \quad , i = 1,2 \tag{22}$$

where the V_{DC_i} is the DC component and V_{RF_i} the radio signal. The MZIM used on the experimental validation was the single-drive MZIM, which only use on of the arms. Therefore, there is no driving voltage on arm 1, which means that $V_{DC_1} = 0$, $V_{RF_1} = 0$, $V_{DC_2} = V_{DC}$ and $V_{RF_2} = V_{RF}$.

Thus, the optical field at the output can be expressed as

$$\begin{aligned} E_{out}(t) &= \frac{E_{in}(t)}{2}\left[1 + e^{j\pi\frac{V_{DC}+V_{RF}}{V_\pi}}\right] \\ &= E_{in}(t)cos\left[\frac{\pi}{2}\frac{V_{DC}+V_{RF}}{V_\pi}\right]e^{-j\frac{\pi V_{DC}+V_{RF}}{2\ V_\pi}} \end{aligned} \tag{23}$$

where V_π is the voltage needed to introduce a phase shift of π.

In a MZIM an optical double side band format is generated. Moreover, MZIM implies that the RF signal applied is real, which means that the OFDM signal must be carried to an intermediate frequency through an IQ modulator. Therefore, the data also appears at the other harmonics on both sides of the carrier.

4.3.2 OPTICAL AMPLIFIER

An optical amplifier is a device used to amplify optical signals without conversion into electrical signal. Yet, during the amplification process, noise is introduced due to spontaneous emission generated photons, which have a power spectral density (PSD) given by

$$S_{ASE} = (G - 1)\, n_{sp} h\, v \tag{24}$$

where ASE stands for Amplified Spontaneous Emission, G is the amplifier gain, n_{sp} represent the spontaneous emission inversion factor, h is the Plank constant and is equal to 6.626×10^{-34}, and v is the optical frequency [3].

4.3.3 PHOTODETECTOR

In the experimental validation tests of the nonlinearity compensation the photodetector used was Lab Buddy. Photodetection are affected by two types of noise: shot noise and thermal noise. The first one is due to the photon fluctuations from the laser or to a so-called dark current, which is the current that flows in the detector when this is not being expose to the light. The second is caused by the carriers fluctuation in the resistance of the photodiode. Similarly to the amplifier noise, the spectral density is considered white noise. However, its effect is considered irrelevant when compared to such.

4.3.4 OPTICAL FIBER CABLE

The optical fiber cable has also some drawbacks that affect the optical signal transmission. The two majors are attenuation and dispersion effects. The optical loss is composed essentially by intrinsic loss, microbending loss and splicing loss. The intrinsic or

material loss is essentially caused by the absorption loss due to hydroxyl groups (OH) impurities and to the microscopic inhomogeneities of the material, called Rayleigh Scaterring loss. Microbending loss is due to the power coupling of the guided fundamental and radiations modes. Lastly, splicing loss results from the axial misalignment of the fiber core, which drastically reduces the unrepeated distance that can be achieved [12]. The attenuation coefficient, α, can be expressed in dB/Km by

$$\alpha = -\frac{10}{L} log_{10}\left(\frac{P_{out}}{P_{in}}\right) \tag{25}$$

The dispersion in optical fiber is defined as the spreading of the light pulse over time. It is divided into material dispersion, waveguide dispersion and modal dispersion. A thorough analysis is made in [12].

The transfer function of the low pass equivalent representation of optical single-mode fiber (SMF) around the optical wavelength λ_c, considering attenuation and the group velocity dispersion (GVD), can be expressed as:

$$H_{fiber}(z, f) = e^{-\frac{\alpha}{2}z} e^{j\pi\frac{Df^2z}{c}} \tag{26}$$

where z is the fiber longitudinal coordinate, c is the free-space speed of light, D is the fiber dispersion parameter usually expressed in *ps/nm/km* and α the attenuation constant usually expressed in *dB/km* [3].

In the experimental setup only small fiber cables (less than 3 meters) were used in the link.

4.4 CHARACTERIZATION OF THE NONLINEAR DISTORTION

Nonlinear distortions present in the fiber can be characterized by several figures of merit. Two of them are the characteristic curves Amplitude to Amplitude (AM/AM) and Amplitude to Phase (AM/PM). The AM/AM characteristic curve represent the distortion of the output power compared to the input power. Unlike to a nonlinear system, in an ideal/linear system, the output power increases linearly with input power. Therefore, in order to compare the difference between the nonlinear and linear systems, a linear curve is present in Fig. 19.

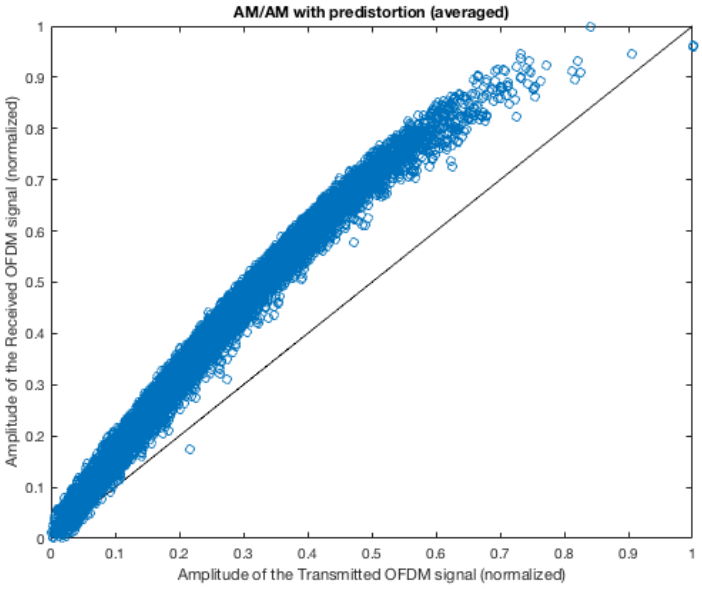

FIGURE 19: AM/AM

The other figure of merit, AM/PM (as shown in Fig. 20), depicts the existent distortion in the phase of the output signal, according to the input power. Here, if there were no distortion (linear system) all the values would be zero.

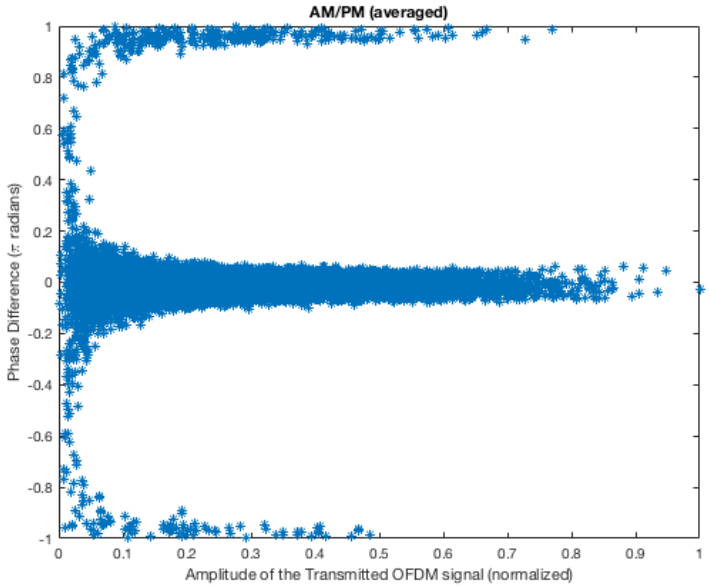

FIGURE 20: AM/PM

4.5 COMPENSATION OF THE NONLINEARITY

The compensation of the nonlinear distortions is accomplished by the implementation of the predistortion algorithm based on a special case of Volterra series analysis model using memory polynomials proposed by J. Kim and K. Konstantinous in [16] depicted in Fig. 21. The predistorter coefficients are calculated in a so-called training phase, and its procedure is explained in [3]. The training block uses an adaptive optimization method to adjust its parameters and, after a considerable number of samples, it is implemented as predistorter [17].

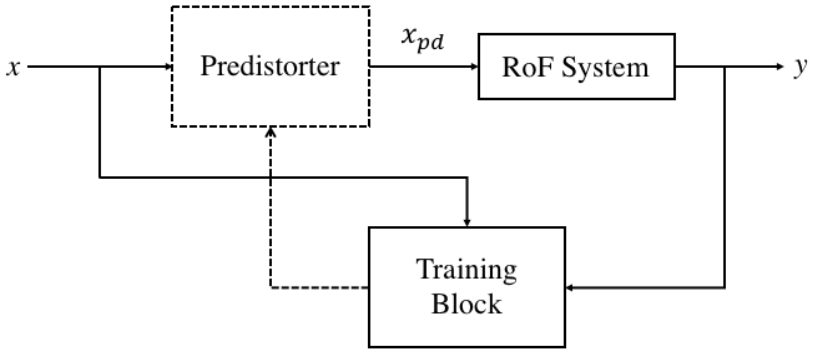

FIGURE 21 – COMPENSATION OF THE NONLINEARITY.SOURCE: [29]

The signal *x* represents the OFDM transmitted signal at an intermediate frequency, y the OFDM received signal and $x_{pd}$the signal after the coefficients are applied, which is give as

$$x_{pd} = \sum_{k=1}^{K} \sum_{q=1}^{Q} a_{kq}\, x(n-q) \mid x(n-q) \mid^{k-1} \tag{27}$$

where K represents the nonlinear order and Q the memory depth of the mathematical model. These should optimize in order to provide the best performance of the predistorter system. Note that only odd orders should be chosen for k, since the system is not substantially improved with even values [3].

5. EXPERIMENTAL VALIDATION

This chapter is the main focus of the dissertation. Parameters are defined for electrical and RoF systems tests. First, the limitations of the RF equipment are identified, an OFDM signal is generated transmitted and received, its performance is evaluated in terms of EVM, different constellation parameters are considered. In the second part experimental validation of the compensation of the RoF system nonlinearities by means of digital predistortion algorithms implemented in [3] is carried out.

5.1 ELECTRICAL EXPERIMENTAL SYSTEM EVALUATION

The objective of the electrical system tests is to understand the performance of the electrical part of the RoF system and its limitations. In other words, the objective is to identify the maximum QAM modulation order (M), for certain conditions and parameters, that provides a back to back RF system performance, within the EVM limit. The EVM limit corresponding to a bit error rate (BER) of 10^{-3} for which Forward Error Correction (FEC) can reduce the BER to 10^{-12}.

5.1.1 EXPERIMENTAL SETUP

The electrical laboratory setup is illustrated in Fig. 22.

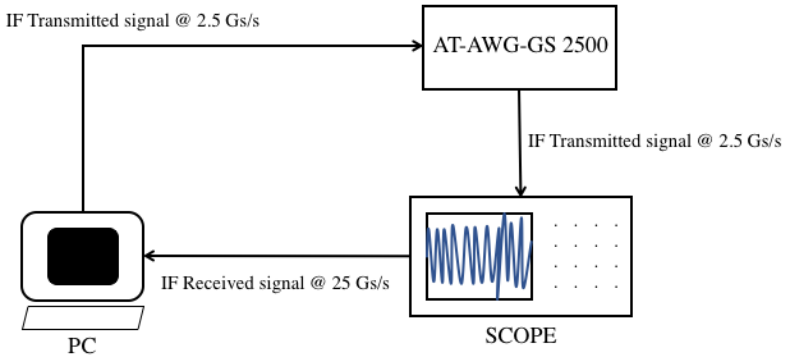

FIGURE 22 – ELECTRICAL EXPERIMENTAL SCHEME

For the electrical system tests, the transmission and reception of the electrical signal was implemented on PC/laptop by means of two Matlab functions. The Transmitter function generates a sequence of bits that are modulated using OFDM modulation. The OFDM signal is generated with a 2.5 GHz sample frequency (Fs). After that is up-converted to an intermediate frequency (IF), f_{IF}. The IF signal is uploaded in the signal generator AT-AWG-GS 2500 and received by the scope (Tektronix DPO 70404). The receiver function collects the signal in the scope at 25 Gsamples/s and apply the demodulation process. Since the scope and the signal generator operate at different frequencies, an external clock is connected between them in order to reduce the frequency offset and phase noise. It was also used the DC Direct output of the signal generator because was the one that introduces less interference.

5.1.2 EQUIPMENT MAIN FEATURES

In this subsection are identify the main features of the experimental equipment to consider for the evaluation of the electrical system performance.

5.1.2.1 AT-AWG-GS 2500

The principal characteristics of the signal generator are:

- Analog outputs:Direct DAC:Bandwidth: 1GHz (calculated @ 500 mVpp SE); dynamic range: 800 mVpp SE, 1.6 Vpp Diff
- DC Amplified:Bandwidth: 600 MHz (calculated @ 1 Vpp SE); dynamic range: 2 Vpp SE, 4 Vpp Diff

The DC Amplified has a hardware filter (-3 dB @ 900 MHz) that can be used to improve harmonic or non-harmonic distortions at higher frequency rates and to reduce sampling clock spurs. [18]

- External clock: Maximum sampling clock frequency is 2.5 GHz
- Sample rate: 2.5 Gsamples/s
- 14 bits DAC

5.1.2.2 TEKTRONIX DPO 70404

The main characteristics of the scope are: analog bandwidth of 4GHz, analog sample rate-25 Gsamples/s and memory - 10 M samples.

5.1.3 EXPERIMENTAL CAPABILITIES

In order to evaluate the system performance, was considered an intermediate frequency of 625 MHz, which is the maximum frequency allowed for a 2.5 Gsamples/s operation. The parameters that were varied to identify the maximum order of constellation were: the **samples per symbol** (sps) of the SRRC filter applied (which affects the bit rate through the equation $R_{bit} = \frac{Fs}{sps}\, n$, where n is the number of bits per symbol), **number of subcarriers** and number of **OFDM symbols**, so that the 5 M samples are not exceeded. The results are presented in TABLE 1.

Samples Per symbol (SPS)	Bit Rate (Gbps)	Number of OFDM symbols	Number of Subcarriers	Maximum Constellation Order (M)
4	5	800	64	256
	5	640	128	256
	5	320	256	256
	4.375	160	512	128
	4.375	80	1024	128
8	2.8125	640	64	512 (↑)
	2.8125	320	128	512 (↑)
	2.8125	160	256	512 (↑)
	2.5	80	512	256 (↑)
	2.1875	40	1024	128
16	1.5625	300	64	1024 (↑)
	1.4063	150	128	512
	1.4063	80	256	512
	1.25	40	512	256
	0.9375	20	1024	64 (↓)

TABLE 1: MAXIMUM CONSTELLATION ORDER ACCODING WITH OFDM PARAMETERS

Since the constellation order decreased for 1024 subcarriers and for rate close to 1 Gbps, it was decided to assess for what debts the remaining constellation orders were decreasing according to the number of carriers. The obtained results are shown in the table below (TABLE 2):

Samples Per symbol (SPS)	**Number of OFDM symbols**	**Number of Subcarriers**	**Maximum Constellation Order (M)**	**Bit Rate (Gbps)**
20	30	512	128 (↓)	0.875
28	45	256	256 (↓)	0,7143
64	60	128	256 (↓)	0,3125
96	40	64	512 (↓)	0,2604

TABLE 2: BIT RATE VALUES FOR WHICH THE CONSTELLATION ORDER DECREASES

These results were taken into consideration in the choice of the parameters for the tests performed in the experimental validation of the nonlinearity compensation.

5.2 EXPERIMENTAL VALIDATION OF THE NON-LINEARITY COMPENSATION

5.2.1 EXPERIMENTAL SETUP

The laboratory setup is shown in Fig. 23 and Fig.24, where the components are identified.

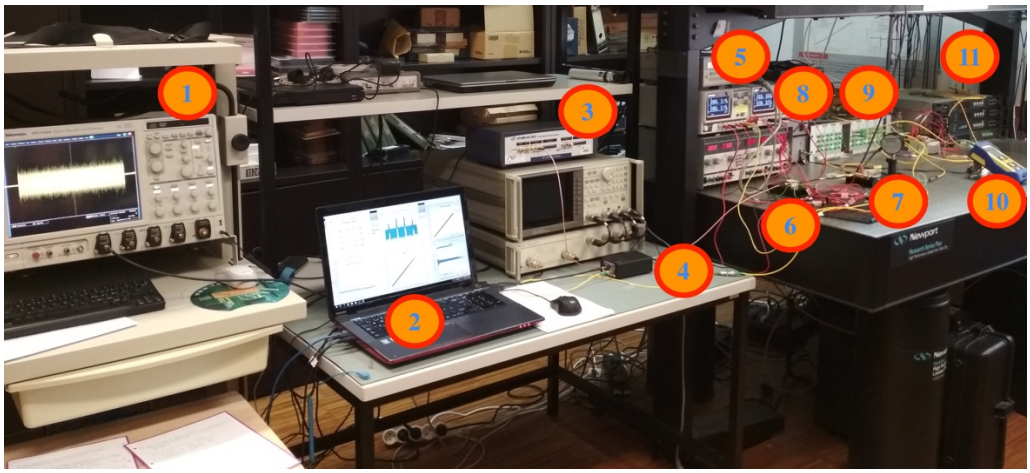

FIGURE 23: EXPERIMENTAL SETUP

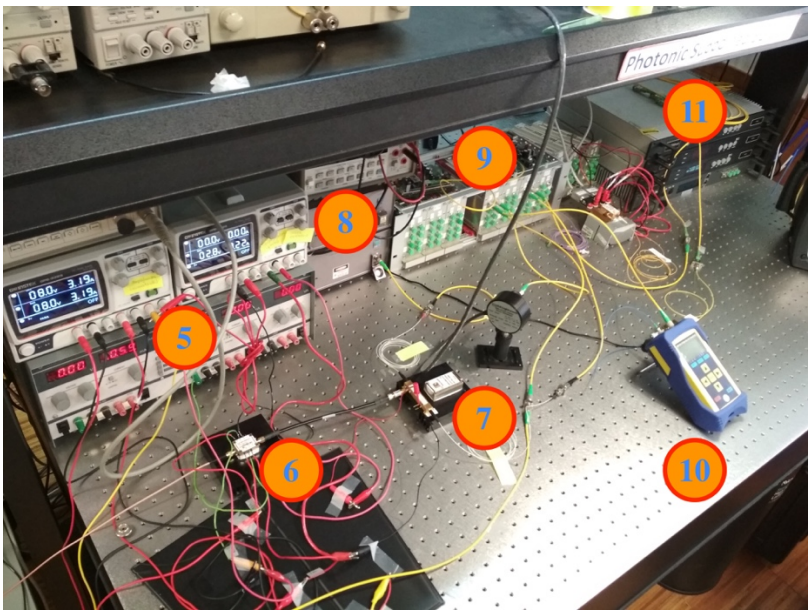

FIGURA 24: OPTICAL SYSTEM SETUP

The components identified are:

1. Scope
2. PC/laptop
3. AT-AWG-GS 2500
4. Photodetector
5. DC sources
6. Optical Modulator Driver
7. Mach-Zehnder Intensity Modulator
8. Laser
9. Power splitter (50%)
10. Attenuator
11. Optical Amplifier

To analyze the RoF experimental link performance, it was also used Matlab functions for the transmission and reception. Similarly to the electrical tests, the OFDM signal is sent to the optical system through the signal generator. The signal modulates the laser by means of MZIM. The Mach-Zehnder modulator is connected to the optical amplifier by an isolator in order to avoid reflections. The modulated optical signal is amplified and filtered. Following, the power of the signal is attenuated and then equally split; one is used for monitoring the power, whereas the other goes to the photodetector to be converted into an electrical signal and sent to the scope. The receiver function collects the signal from the scope using a cycle with 10 iterations to get a considerable number of samples, with about 4 000 000 in each iteration. The demodulation process is achieved and the coefficients of the predistortion method are calculated. Then the all process is repeated, but, this time, the coefficients are applied to the signal to be transmitted and the receiver analyze the improvement of the system performance.

A scheme of the RoF experimental system is depicted in Fig. 25. A power balance of the setup was achieved, and the points of interest are indicated in the figure. The power measured are: $P_1 = -7\ dBm;\ P_2 = 11\ dBmP_3 = 14\ dBm;\ P_4 = -14.56\ dBm$ and $P_5 = -19.09\ dBm$.

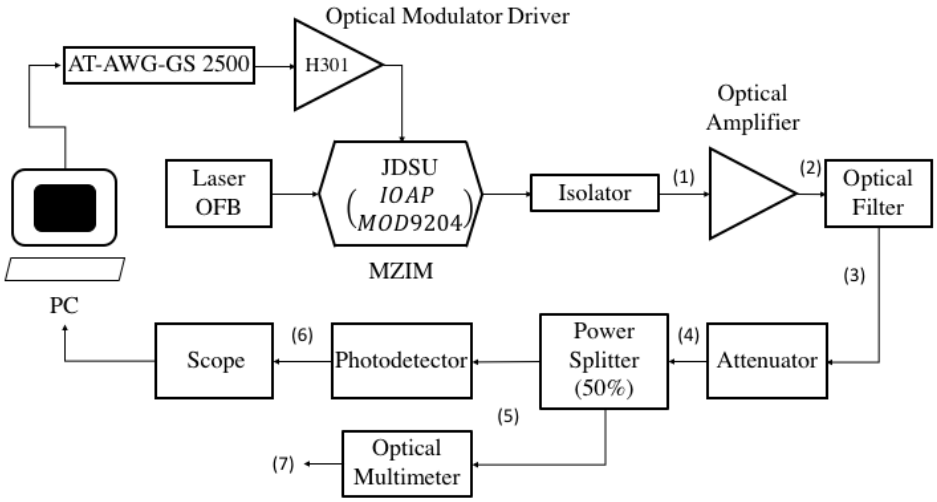

FIGURE 25 - ROF EXPERIMENTAL SCHEME

The optical amplifier (OA) has a gain of 17 dB and the optical filter (OF) attenuates 3 dB. Considering that the maximum power allowed in the photodetector is P_{max}= 4dBm, attenuation was introduced in the link, so that the output power of PD is 0 dBm. The power measured in PD was P_6= 0.06 dBm and in the optical multimeter was P_7= 0.33 dBm, which means that the cable connected to the PD has an attenuation of 0.27 dB.

Some components of the system were characterized. First a measurement of the optical DC transfer characteristics of the MZIM was performed in order to obtain the value of V_π. The curve obtained is shown in Fig. 26.

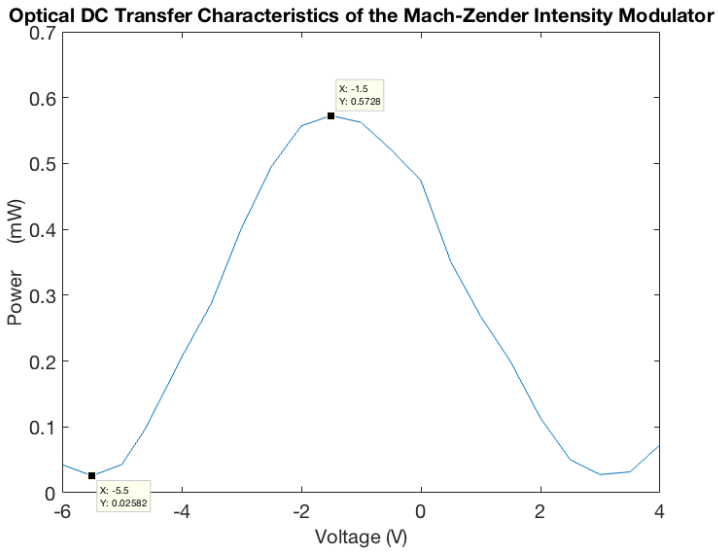

FIGURE 26 – OPTICAL DC TRANSFER CHARACTERISTICS OF THE MACH-ZEHNDER INTENSITY MODULATOR

The maximum bias voltage of the MZIM is $|V_{bias}| = 4\,V$, however the peak of the curve is at -1.5 V instead of 0 V. Thus, the study was made until -6 V. The minimum voltage measured was -5.5 V. Therefore, the voltage needed to introduce a phase shift of π is $V_\pi = |-5.5| - |-1.5| = 3.5\,V$.

Fig. 27 shows the optical spectrum of the laser which is centered at λ = 1550,9 nm, and the peak power is -1 dBm.

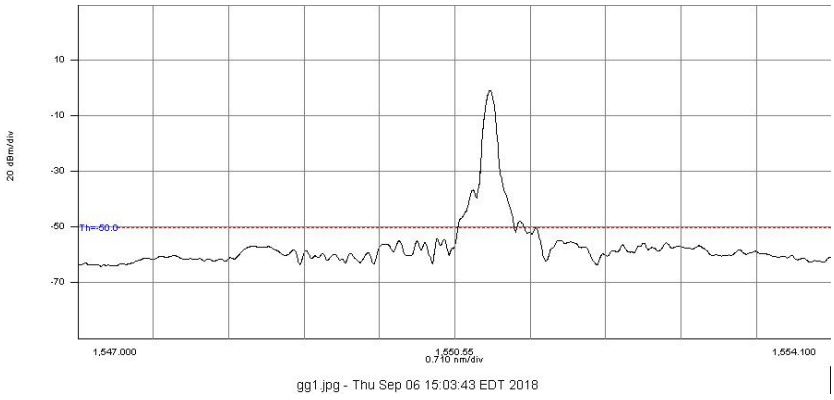

FIGURE 27 – LASER POWER SPECTRUM

The key features of the optical modulator driver (Model H301) are: **data rate** - from 2.488 to 12.2 Gb/s; **maximum output amplitude** - 7.5 Vpp; **Gain** - 14 to 24 dB, variable; **P_{sat} output**- 4 dBm

5.2.4 EXPERIMENTAL CHARACTERIZATION OF THE SYSTEM NONLINEARITIES

As mention before, the characterization of the nonlinear distortions can be accomplished by means of AM/AM and AM/PM curves. It was considered three levels of distortion according to the amplitude percentage of the OFDM signal that is sent by the signal generator. The percentages considered were 50, 75 and 100. The following figures

(28-33) depict the nonlinear distortions characterization for the tree levels (blue curves) as well as the measured pre-distorted curves (red curves). The straight line corresponds to an ideal system.

Amplitude (%) = 50

AM/AM

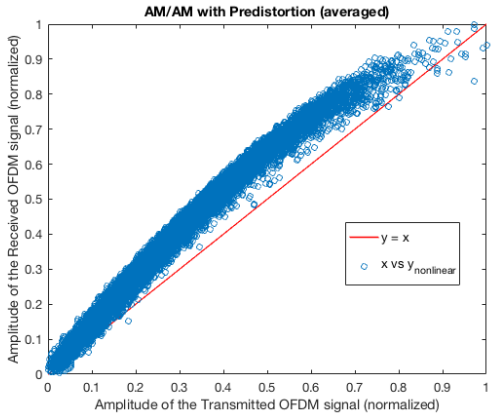

FIGURE 28: AM/AM FOR AMPLITUDE (%) = 50

AM/PM

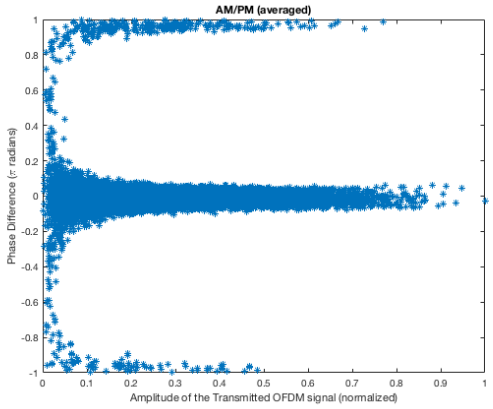

FIGURE 29: AM/PM FOR AMPLITUDE (%) = 50

Amplitude (%) = 75

AM/AM

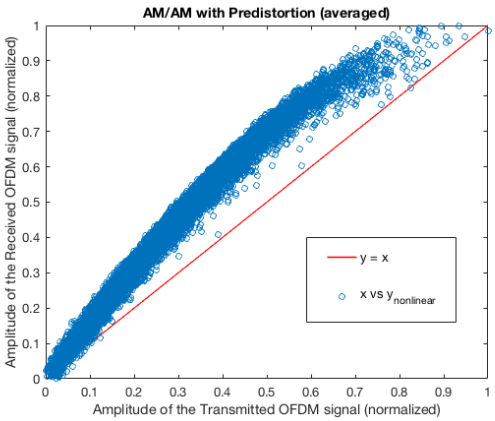

FIGURE 30: AM/AM FOR AMPLITUDE (%) = 75

AM/PM

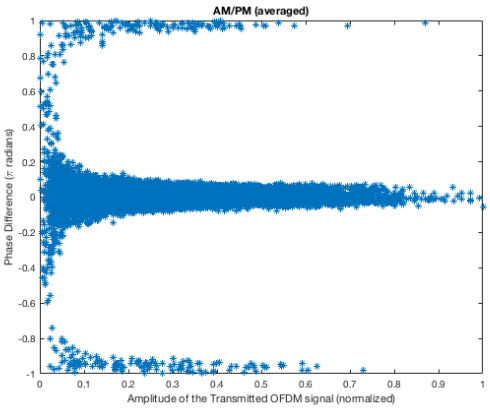

FIGURE 31: AM/PM FOR AMPLITUDE (%) = 75

Amplitude (%) = 100

AM/AM

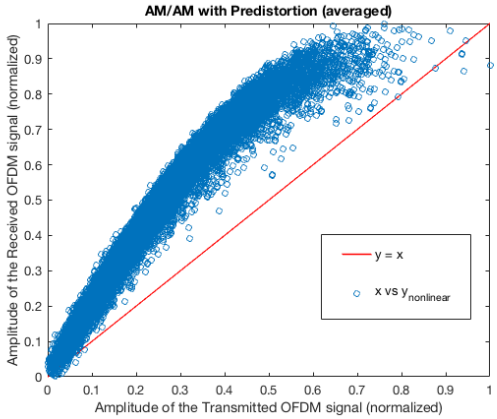

FIGURE 32: AM/AM FOR AMPLITUDE (%) = 100

AM/PM

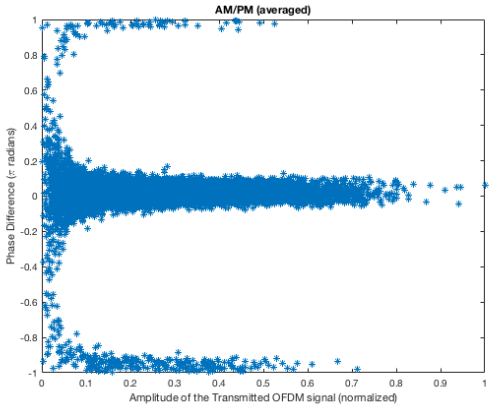

FIGURE 33: AM/PM FOR AMPLITUDE (%) = 100

5.2.5 DISTORTION COMPENSATION

The compensation of the nonlinear distortions was performed in two parts: training phase and implementation of the predistortion. In the training phase, an OFDM signal carried at IF = 625 MHz, x, was generated and send to the RoF system through the signal generator AT-AWG-GS 2500. The receiver function collects the electrical signal from the scope and applied the functions of the predistortion algorithm to calculate and optimize the coefficients of the memory polynomials. This process is illustrated in Fig.34.

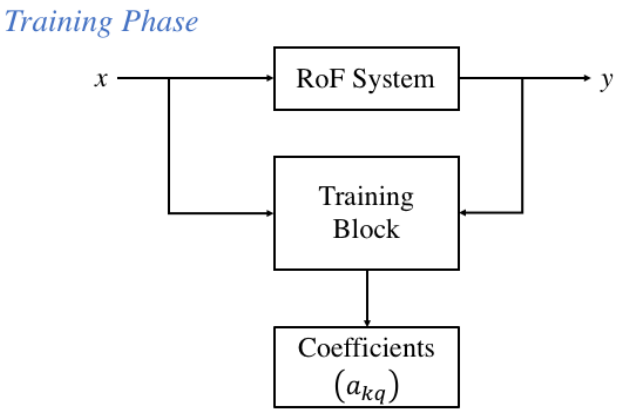

FIGURE 34: PREDISTORTER TRAINING PHASE

After the optimization of the coefficients is complete, the predistorter is implemented. Here, a new OFDM signal is generated by the same function used in the training phase and send to the RoF system also via the signal generator. The received OFDM signal is collected and saved. Thereafter, a different transmitter function applies the coefficients to the signal used in the previous transmission and send the predistorted signal to RoF system. A different receiver function is also used, where the demodulation process is identical, however, with the addition of a comparison between the received signal with and without predistortion. This improvement analysis is accomplished by means of AM/AM and AM/PM curves, and constellation diagrams. A simple representation of the predistortion implementation procedure is shown in Fig. 35.

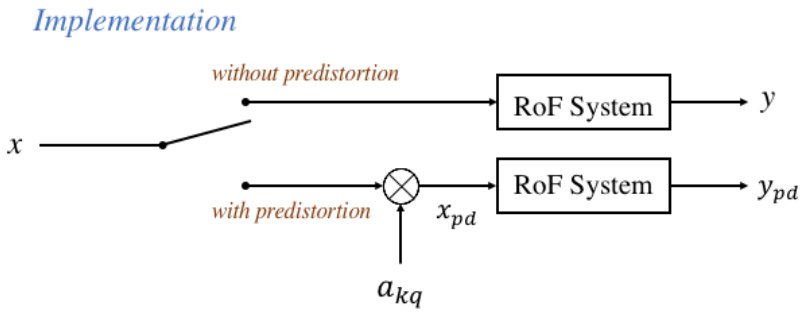

FIGURE 35 – PREDISTORTER IMPLEMENTATION PHASE

5.2.6 OPTIMIZATION OF THE MEMORY POLYNOMIALS FOR THE DIFFERENT LEVELS OF DISTORTION

In order to improve the system performance, an optimization of the memory polynomials was achieved by the selection of K e Q for the different levels of distortion. The OFDM parameters chosen for the optimization are indicated in Table 3.

Parameters	Values
Intermediate Frequency (IF)	625 MHz
Constellation order (M)	16
Number of Subcarriers	128
Samples per symbol (SPS)	16
Bit Rate	625 Mbps
Number of OFDM symbols	160

TABLE 3: OFDM PARAMETERS

The results of the optimization for each level of distortion are presented in the table below:

Amplitude (%)	Order Of Nonlinearity (K)	Memory Depth (Q)	EVM without predistortion (dB)	EVM with predistortion (dB)
50	5	2	-29.1	-34.3
75	5	2	-22.7	-31.5
100	5	5	-17.9	-28.8

TABLE 4: OPTIMIZED COEFFICIENTS ACCORDING WITH THE LEVEL OF DISTORTION

The results indicate that the system has more EVM improvement with the 75% and 100% amplitude levels. Although there was an improvement in amplitude, the phase noise remains.

Since the latter has a huge level of distortion, the 75% amplitude level was the chosen one to analyze the system with predistortion for different values of constellation order.

5.2.7 IMPROVED SYSTEM PERFORMANCE FOR DIFFERENT VALUES OF CONSTELLATION ORDER

The OFDM parameters chosen for the analysis of predistortion implementation for different values of M were the same as the ones used for the optimization tests. The results are shown in the following table (Table 5):

Constellation Order (M)	**EVM without predistortion (dB)**	**EVM with predistortion (dB)**	**FEC Limit (dB)**
16	-22.72	-31.54	-12.94
32	-21.51	-30.42	-16.03
64	-20.5	-29.21	-19.05
128	-21.54	-31.21	-22.03
256	-20.8	-30.28	-24.99
512	-18.67	-28.17	-30.92

TABLE 5: IMPROVEMENT OF THE SYSTEM PERFORMANCE FOR DIFFERENT CONSTELLATION ORDER

For the chosen OFDM parameters, the results show that only for M=512 the EVM of the improved system remains above of the FEC limit. Therefore, for this case errors cannot be corrected. In order to illustrate the system operation with digital pre-distortion several representative system performance metrics are shown in Figs. 36-39.

AM/AM

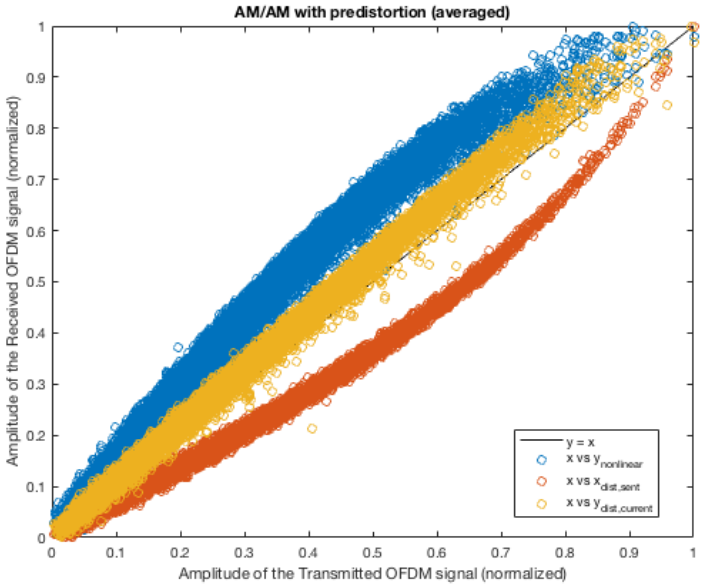

FIGURE 36 – AM/AM FOR M = 64

The amplitude of the received signal without predistortion is the blue curve, the predistortion signal is the orange and the signal with predistortion is the yellow. It can be seen that with the implementation of the predistortion the signal became closer to the ideal/linear.

AM/PM

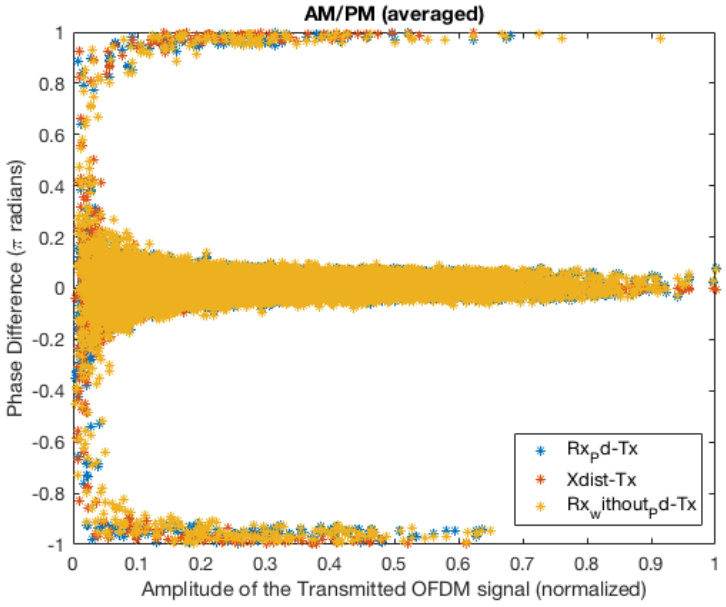

FIGURE 37 – AM/PM FOR M = 64

Similarly to the AM/AM characterization, the phase of the received signal without pre-distortion is the blue curve, the predistortion signal is the orange and the signal with pre-distortion is the yellow. In spite of the improvement of the system performance, the phase noise introduced by the system remains, even though small.

EVM

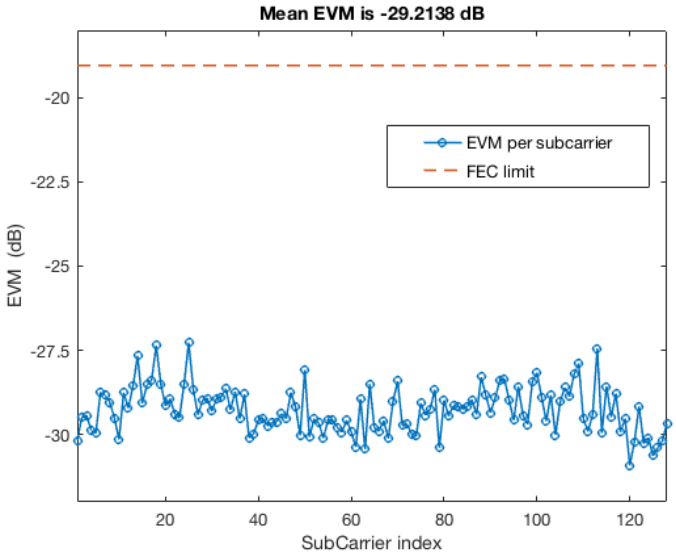

FIGURE 38 – EVM FOR M= 64

Besides the fact that the previous EVM for this constellation order is not present in the figure, Table 5 indicates that its value is -20.5 dB. This means that the EVM had an up-grading of nearly 10 dB.

Constellation Diagram

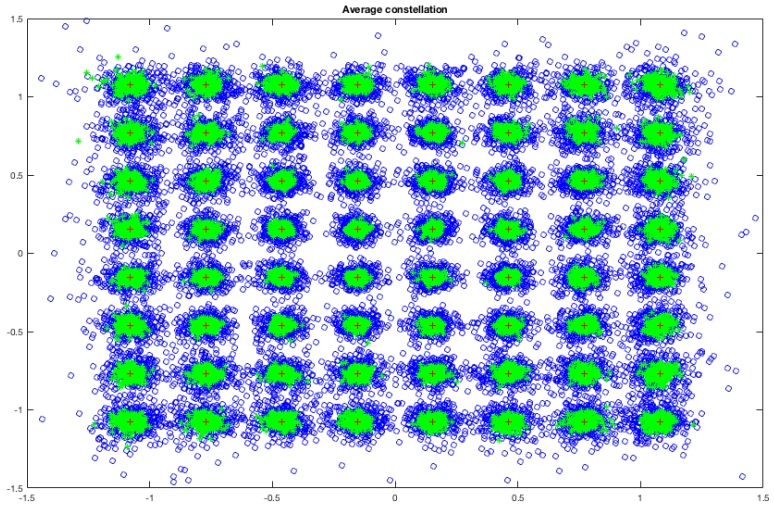

FIGURE 39 – CONSTELLATION DIAGRAM FOR M =64

The blue dots are the constellation points without predistortion, whereas the green ones are the constellation points with predistortion. It can be seen that the cloud of the pre-distortion points are closer of the ideal point, which indicates a considerable improvement in the system.

6. CONCLUSION

In this latter chapter, the conclusions of the experimental validation work are discussed in the first section. The second section presents suggestions of future work.

6.1 CONCLUSIONS

The aim of this dissertation was the experimental validation of nonlinear effects compensation in RoF systems. This compensation technique was accomplished by means of predistortion algorithm based on memory polynomials. A study of the OFDM system was carried out in order to understand its limitations in terms of constellation order. Upper and lower limits were defined according with the samples per symbol of the SRRC filter, since this parameter directly affects the bit rate. The maximum M achieved was 1024, for 64 carriers and 1.5625 Gbps, whereas the minimum was 64, for 1024 carriers and 0.9375 Gbps. We concluded that, in a real environment the use of a bit rate around the 1Gps is more reliable. These results were helpful to select the OFDM parameters for the analysis of the optical link.

The main goal of this dissertation is the experimental validation of the compensation of the RoF system nonlinearities by means of predistortion implemented in [3]. The experimental validation methodology will be divided in two parts. In first place, a study of the limitations of the OFDM system transmission in terms of constellation order will be carried out, according with the variation of certain parameters such as number of carriers, number of OFDM symbols and samples per symbol of the filter, which directly affect the bit rate. It will also be chosen an intermediate frequency (IF) to carry the OFDM signal. This study is helpful to select reliable parameters for the second part. Here, the OFDM signal modulates a continuous wave (CW) by means of a Single-Driver Mach-Zehnder

Intensity Modulator. The distortions introduced by the RoF link are identified and characterized, and the improvement of system performance with predistortion algorithm developed in [3] is analyzed.

in

In [3] the compensation of the RoF system nonlinearities by means of digital predistortion was implemented. The predistortion method was analyzed for several system parameters, such as number of bits per symbol, bit rate and fiber length. It was verified that either for AM/AM or AM/PM the predistortion can compensate the nonlinear distortions. In this dissertation, a laboratory setup to test the predistortion method was assembled. Using this experimental setup the predistortion method was experimentally validated. The experimental validation was assessed for different OFDM signals, for fixed RF carrier and various constellation order. Under these conditions, the predistortion algorithm proved to be valid in a real environment. Although, unlike [3], the AM/PM curve was not compensated, i.e., the phase noise introduced by the system, even small, was not completely compensated.

6.2 FUTURE WORK

The suggestions for future work are:

- Implementation of a graphical user interface
- Experimental study with different OFDM parameter, including intermediate frequency
- Experimental analysis of the fiber length impact
- Experimental study in order to improve the phase noise

REFERENCES

[1] P. Monteiro and A. Gameiro, “Convergence of Optical and Wireless Technologies for 5G,” in *Opportunities in 5G Networks*, F. Hu, Ed. CRC Press, 2016, pp. 179–215.

[2] Y. Niu *et al*., “A survey of millimeter wave communications (mmWave) for 5G: opportunities and challenges,” *Wirel. Networks*, vol. 21, no. 8, pp. 2657–2676, Nov. 2015.

[3] Beatriz Manata de Oliveira (September 2017), “Performance Analysis of radio over fiber systems employing digital predistortion”. Dissertation submitted in partial fulfillment of the requirements for the degree of Master of Science in Electrical and Computer Engineering.

[4] A. Hekkala *et al*., “Predistortion of Radio Over Fiber Links: Algorithms, Implementation, and Measurements,” *IEEE Trans. Circuits Syst. I Regul. Pap*., vol. 59, no. 3, pp. 664–672, Mar. 2012.

[5] Isiaka Ajewale Alimi, António Luís Teixeira and Paulo Pereira Monteiro, “Towards an Efficient C-RAN Optical Fronthaul for the Future Networks: A Tutorial on Technologies, Requirements, Challenges, and Solutions”, IEEE Communication surveys & tutorials

[6] J. C. Z. Jeffrey G. Andrew, Stefano Buzzi, Wan Choi, Stephen V. Hanly, Angel Lozano, Anthony C. K. Soong, “What Will 5G Be?,” *IEEE J. Sel. Areas Commun. Top. Quantum Electron*., vol. 32, no. 6, pp. 1065–1083, 2014

[7] Yong Soo Cho *et al*., *MIMO-OFDM Wireless Communications with MATLAB*, 2010

[8] R. Van Nee and R. Prasad, *OFDM For Wireless Multimedia Communications*. Artech House, Inc., 2000.

[9] Dr. Raymond McArthur,” Intermodulation Fundamentals” [Online] Available: “http://www.sinctech.com/wp-content/uploads/2012/10/final.pdf [Accessed: 20-July-2018]

[10] R. A. Shafik, M. S. Rahman, and A. H. M. R. Islam, “On the extended relationships among EVM, BER and SNR as performance metrics,” *Proc. 4th Int. Conf. Electr. Comput. Eng. ICECE 2006*, no. December, pp. 408–411, 2007.

[11] V. A. Thomas, M. El-Hajjar and L. Hanzo, "Millimeter-Wave Radio Over Fiber Optical Upconversion Techniques Relying on Link Nonlinearity," in *IEEE Communications Surveys & Tutorials*, vol. 18, no. 1, pp. 29-53, Firstquarter 2016

[12] Le Nguyen Binh, *Optical Fiber Communication Systems with MATLAB and Simulink models*. 2nd Edition

[13] John E. Mitchell, "Integrated Wireless Backhaul Over Optical Access Networks" , Journal of lightwave technology, vol. 32, no. 20, October 15, 2014

[14] The Physics classroom, "Doppler Effect". [Online] Avaiable: https://www.physicsclassroom.com/class/waves/Lesson-3/The-Doppler-Effect. [Accessed: 23-Ag-2018]

[15] Jo Best, "Tech Republic: The race to 5G: Inside the fight for the future of mobile as we know it" [Online]. Available: https://www.techrepublic.com/article/does-the-world-really-need-5g/. [Accessed: 8-July-2018].

[16] J. Kim and K. Konstantinou, "Digital predistortion of wideband signals based on power amplifier model with memory", Electron. Lett., vol. 37, no. 23, pp. 1417–1418, Nov. 2001

[17] A. Hekkala, "Predistortion of Radio Over Fiber Links: Algorithms, Implementation, and Measurements," *IEEE Trans. Circuits Syst. I Regul. Pap.*, vol. 59, no. 3, pp. 664–672, Mar. 2012

[18] Active Technologies S.r.I, "AT-AWG-GS 2500 user manual", Rev 1.3, September 2013.

[19] E. Hossain and M. Hasan, "5G cellular: key enabling technologies and research challenges," *IEEE Instrum. Meas. Mag.*, vol. 18, no. 3, pp. 11–21, Jun. 2015

[20] Isiaka Akewale Alimi (2017), "Optimization of Optical Fronthaul for Cloud Computing Radio Access Networks (CC-RAN)". Thesis submitted to the Universidade do Minho, Aveiro and Porto in partial fulfillment of the requirements for Doctoral Degree in Engenharia Electrotécnica/Telecomunicalções under the MAP-Tele doctoral program.

[21] Product Bulletin, "JDS Uniphase 10 Gb/s Amplitude Modulator"

[22] Product Bulletin, "JDS Uniphase 10 Gb/s Amplitude Modulator Driver – H301 series"

[23] W. Shieh and I. Djordjevic, *OFDM for Optical Communications*. Elsevier Inc., 2010.

[24] L. Ding *et al.*, "A Robust Digital Baseband Predistorter Constructed Using Memory Polynomials," *IEEE Trans. Commun.*, vol. 52, no. 1, pp. 159–165, Jan. 2004.

[25] Taewon Hwang *et al*, "Transactions on Vehicular Technology", IEEE, vol.: 58, Issue: 4, May 2009

[26] Imec,"60GHz technology for Wigi and 5G applications" [Online]. Available: https://www.imec-int.com/cache/pdfs/en/imec-magazine/imec-magazine-april-2017/60ghz-technology-for-wigig-and-5g-applications.pdf [Accessed: 15-August-2018].

[27] Abdelhakim Boudkhi, Asmaâ Ouzzani and Belabbes Soudini, "Analysis of Fundamental Photodetection Noises and Evaluation of PIN and APD Photodiodes Performances using an Optical High Debit Transmission Chain Simulated by Optisystem" , International Journal of Computer Applications (0975 – 8887), Volume 115 – No. 18, April 2015 .

[28] A. Bruce Carlson and Paul B. Crilly, *Communication Systems*. 5th Edition

[29] S. R. Abdollahi *et al*., "Digital Radio over Fibre for Future Broadband Wireless Access Network Solution"